frontiers | Frontiers in Earth Science

TYPE Original Research
PUBLISHED 17 July 2024
DOI 10.3389/feart.2024.1410585

OPEN ACCESS

EDITED BY
Sung Keun Lee,
Seoul National University, Republic of Korea

REVIEWED BY
Sun Young Park,
Korea Institute of Geoscience and Mineral Resources, Republic of Korea
Kyung Jae Lee,
University of Houston, United States

*CORRESPONDENCE
Wei Yang,
yangw@pku.edu.cn

RECEIVED 01 April 2024
ACCEPTED 28 June 2024
PUBLISHED 17 July 2024

CITATION
Yang W, Shen B, Zhang Z, Zhao R, Hou H, Li Z, Ding M, Hu H, Feng F and Xie M (2024), Comparative study on pore-connectivity and wettability characteristics of the fresh-water and saline lacustrine tuffaceous shales: triggering mechanisms and multi-scale models for differential reservoir-forming patterns.
Front. Earth Sci. 12:1410585.
doi: 10.3389/feart.2024.1410585

Comparative study on pore-connectivity and wettability characteristics of the fresh-water and saline lacustrine tuffaceous shales: triggering mechanisms and multi-scale models for differential reservoir-forming patterns

Wei Yang[1,2]*, Baojian Shen[1,3], Zilong Zhang[2], Rui Zhao[1,4], Haodong Hou[2], Zhiming Li[1,3], Mou Ding[2], Hanwen Hu[3], Fan Feng[3] and Ming Xie[2]

[1]State Key Laboratory of Shale Oil and Gas Enrichment Mechanisms and Effective Development, Beijing, China, [2]Unconventional Oil and Gas Research Institute, China University of Petroleum, Beijing, China, [3]Sinopec Petroleum Exploration and Production Research Institute, Beijing, China, [4]China Petroleum & Chemical Corporation, Beijing, China

Although particular attention has been paid to responses of hydrocarbon storage and percolation capacity to the devitrification concerning lacustrine tuffaceous shale reservoirs in recent years, there is still a lack of systematical and comparative investigation on differential patterns and potential triggering mechanisms concerning development of the pore-microfracture systems and characteristics of surface wettability between the fresh-water and saline lacustrine settings, which is of considerable importance in fully understanding of genesis and spatial distribution of dessert reservoir intervals of tuffaceous shale reservoirs, and to provide further conceptual basis for deciphering shale-oil movability of saline lacustrine fine-grained mixed sedimentary sequences. In this study, tuffaceous shales from both the Upper Triassic Yanchang Formation in the Ordos Basin and Middle Permian Jingjingzigou Formation in the Junggar Basin are targeted to unravel the differential behavior of tuff devitrification and potential impacts on reservoir wettability and pore connectivity concerning fresh-water and saline lacustrine settings, and we present new results here from integrated analyses and combined interpretation of FE-SEM, Image Pro Plus (IPP) software image processing, contact angle and spontaneous imbibition experiments. In view of comparative analysis from representative samples, the tuffaceous shales from saline lacustrine environments are characterized by well-developed intergranular-intercrystalline and dissolution pores, and inorganic microfractures, generally yield a higher plane porosity of representative pore-fracture spaces and spontaneous imbibition slopes, a relatively lower average of n-decane contact angles and corresponding wettability parameters. The saline lacustrine tuffaceous shales

are thus suspected to have undergone more intense devitrification resulting in a higher amount of devitrification and associated dissolution pores, and a relatively better connectivity between isolated micropore systems with adjacent microfractures. This would significantly facilitate the interface wettability reversal and occurrence of movable hydrocarbon fluid in microscopic reservoir spaces. Finally, a comprehensive and conceptual model is established illustrating the effects of differential devitrification on reservoir-forming patterns concerning tuffaceous shales developed in the fresh-water and saline lacustrine settings, respectively. These findings are of great theoretical and practical significance to enrich theory of high-quality reservoir formation and shale-oil accumulation in saline lacustrine tuffaceous shale reservoirs, and lay the foundation for guiding efficient exploration of continental fine-grained mixed sedimentary sequences.

KEYWORDS

tuffaceous shale, devitrification, pore connectivity, wettability, saline lacustrine, fine-grained mixed sedimentary sequences

1 Introduction

Tuffaceous reservoirs, which are closely related to volcanic activity, have become one of the current research hotspots in the field of earth sciences (Zhu et al., 2019; Zhao et al., 2020). Volcanic activity is instantaneous and isochronous, and the volcanic ash erupted during volcanic activity is also instantaneous and isochronous during deposition, so volcanic ash is widely distributed in various sedimentary basins with distinctive characteristics (Desmastes et al., 2007). Volcanic ash is rich in nutrients, such as, Fe, P, and Ca, which are capable of promoting algae blooms and resulting in high-quality hydrocarbon source rocks in lacustrine sedimentary basins (Liang et al., 2021; Liu et al., 2022; Li et al., 2022). Tuffs can also be used to reconstruct surrounding tectonic magmatic geological events (Wang et al., 2017; Yang et al., 2019; Tian et al., 2022), as well as to clarify the timing and sequence of development of geological events and to restore paleoenvironments (Lowe, 2011). In addition, tuffs can be used as oil and gas reservoirs, and tuff-bearing reservoirs usually have favorable hydrocarbon indications, and high industrial gas flows and industrial oil flows can be seen in tuff-bearing reservoirs in some developed areas, such as the Akita and Niigata basins in Japan (Tomaru et al., 2009), the Richland field in the United States (Zhang et al., 2010), the Neuquén Basin in Argentina (Stinco and Barredo, 2021), the Junggar Basin in China (Zhang et al., 2021) and the Ordos Basin (Wang et al., 2021), among others. In recent years, the research on tuffs or tuff-bearing reservoirs has become a hot topic, mainly focusing on their lithological characteristics, reservoir spatial types and features, and physical properties (Chen et al., 2014; Wang et al., 2017; Pan et al., 2022). In the exploration and development of unconventional hydrocarbons, tuffs or tuffaceous shales generally have better pore space and imbibition capacity (Liu et al., 2022; Wang et al., 2022), and these tuffs or tuffaceous reservoirs with superior reservoir conditions are mainly affected by devitrification, and the reservoir is more favorable for hydrocarbon enrichment after devitrification (Pan et al., 2022).

Devitrification can be regarded as a kind of recrystallization, which is the process of rearranging the molecules and atoms inside the volcanic tuff that are originally loosely arranged, recrystallizing from vitreous silica to fine quartz, feldspar and other crystals, as well as a process of transforming from unstable to stable components (Chen et al., 2014; Lv et al., 2015; Wang et al., 2017; Pan et al., 2022). And in the process of shifting to the crystalline state, the new minerals formed by the devitrified process are reduced in volume, so that a large number of microporosity can be formed between different mineral particles; the new minerals formed by devitrified will be dissolved under the action of fluids and produce dissolved porosity, therefore, the porosity in the reservoir can be effectively enhanced after devitrification (Zhao et al., 2009). Wettability, as one of the important surface properties of an object, is mainly used to reflect the tendency between solids and liquids. The wettability affects the effect of the interaction between geological fluids and reservoirs (Schembre et al., 2006; Lv et al., 2015). The difference of wettability directly affects the reservoir storage capacity. The contact angle method can measure the wettability of rocks most intuitively and effectively, and fluid flow dispersion on the rock surface can be observed. Spontaneous imbibition is the process by which a wettable fluid in the pores of a rock spontaneously replaces another non-wettable fluid by capillary forces. Through spontaneous imbibition experiments, we are able to obtain the influencing factors of the storage capacity inside the rock, such as, wettability, pore structure, viscosity, and interfacial tension (Gao and Hu, 2016; Zhou et al., 2018; Ye et al., 2019; Zhang et al., 2021). The devitrification of tuffaceous components in the reservoir results in characteristic pore-throat structure with a low pore-throat ratio and corresponding small average apertures) leads to similar capillary forces, facilitating hydrocarbon retention and also contributes to the wettability inversion at the interface of the mixed sedimentary tuffaceous shales (Macquaker and Davies, 2008; Liu et al., 2018; Yang et al., 2020).

Although particular attention has been paid to the responses of hydrocarbon storage and percolation capacity to the devitrification concerning the lacustrine tuffaceous shale reservoirs in recent years, there is still a lack of systematical and comparative investigation on differential patterns and potential triggering mechanisms concerning development of the pore-microfracture systems and characteristics of surface wettability between the fresh-water and saline lacustrine settings, which is of considerable importance in

fully understanding of genesis and spatial distribution of dessert reservoir intervals of tuffaceous shale reservoirs, and to provide further conceptual basis for deciphering shale oil movability of saline lacustrine fine-grained mixed sedimentary sequences.

In order to unravel the differential behavior of tuff devitrification and potential impacts on reservoir wettability and pore connectivity concerning fresh-water and saline lacustrine settings, both tuffaceous shales from both the Upper Triassic Yanchang Formation in the Ordos Basin and Middle Permian Jingjingzigou Formation in the Junggar Basin are targeted in this study, and a combined interpretation of FE-SEM, Image Pro Plus (IPP) software image processing, contact angle and spontaneous imbibition experiments is adopted. Using microscopic observation methods at different scales, the observed pores are described in detail and combined with image processing software to quantitatively analyze many types of devitrified causal pores. By determining the wettability angle and the relative wettability parameters, the wettability of various types of devitrified samples can be identified. To study the transport capacity of organic fluids in devitrified oil-bearing reservoirs through spontaneous imbibition experiments can evaluate the pore connectivity of the reservoirs after devitrification. Finally, on the basis of above achievements, we aim to illustrate potential impacts of differential devitrification, and especially to portray the differential behaviors in wettability and pore connectivity of the tuffaceous shale reservoir due to devitrification concerning the fresh-water and saline lacustrine sedimentary environments. These findings may have important theoretical and practical significance for in-depth study of high-quality unconventional hydrocarbon reservoirs under saline lacustrine settings and reliable prediction of shale oil "sweet spots" distribution in terrigenous fine-grained mixed sedimentary sequences.

2 Geological setting

The Ordos Basin is the second largest sedimentary basin in China, spanning Shaanxi, Gansu, Ningxia, Shanxi and Inner Mongolia, the yellow area shown in the figure is the area of this study (Figure 1A). The Ordos Basin is tectonically located in the southwestern part of the North China Craton, which is a large multi-rotational Craton basin with stable overall lift, the depressional migration (Fu et al., 2015), and the basin structure is relatively simple and can be divided into six tectonic units (Figure 1B): the Yimeng uplift in the north, the Weibei uplift in the south, the Western margin thrust belt and the Tianhuan depression in the west, the Jinxi fault-fold belt in the east, and the Yishan slope in the center (Li, 2004; Tian et al., 2015). The Ordos Basin began to form during the Cambrian period and it has been subjected to superposition of multiple tectonic movements to form the current tectonic pattern (Zhang, 1982). The Ordos Basin is rich in, and the Triassic Yanchang Formation is widely distributed in the basin as the most abundant formation in oil and gas resources. The Yanchang Formation sedimentary began at the end of the Middle Triassic, when the Ordos Basin changed from marine sedimentation to lacustrine sedimentation. Under the influence of tectonic movements, the basin was reformed into a large inland fresh-water lacustrine basin, a set of terrestrial clastic rock system characterized by fluvial-lacustrine facies (Qiu et al., 2015a; Qiu et al., 2015b). The Yanchang Formation is subdivided into 10 substrata (Figure 1C) according to their depositional environment and lithologic combination variations. During the deposition of the Yanchang Formation, the lacustrine basin regressed and expanded significantly due to strong tectonic movements with continuous eruptions of volcanic ash from surrounding volcanic movements spilling into the lacustrine basin. A large number of organic-rich shales and tuffs were deposited under semi-deep to deep lake sedimentary conditions, and tuffs were widely distributed in the Yanchang Formation (Yao et al., 2013; Fu et al., 2020; Fan et al., 2021; Fan et al., 2022). Within the Yanchang Formation, a thick layer of organic-rich shale is mixed with tuff layers where the thickness of individual tuff layers varies from a few millimeters to tens of centimeters, and the total thickness can reach several meters (Tang et al., 2015; Dou et al., 2018).

The Junggar Basin is located in the northern part of the Xinjiang Province with a general isosceles triangle shape, the yellow area shown in the figure is the area of this study (Figure 2A), which is characterized by a narrow southern width in the north and a slope from east to west (Yang et al., 2015). The Junggar Basin has undergone multiple periods of tectonic deformation and superimposed transformation, including the Hercynian, Indochina, Yanshan and Himalayan periods, at the same time alternating extension, extrusion, shearing and other tectonic processes, making the region tectonically complex, with strong stratigraphic folding and the formation of a large number of unequal or isoclinal folds (Wu et al., 2005). Therefore, the Junggar Basin can be divided into six secondary tectonic units (Figure 2B), including the Ulungu depression and the Lvliang uplift in the north, the Central depression in the abdomen, the Western uplift, the Eastern uplift, and the Tianshan Mountain thrust belt in the south (Wu, 1986; Yang et al., 2004). The Middle Permian Jingjingzigou Formation is mainly developed near the foothills of the Bogda Mountains on the southern margin of the Junggar Basin (Figure 2C), in integrated contact with the underlying Ulapo Formation, with continuous transition to the overlying Lucaogou Formation (Wang, 2017). During the Middle Permian, the warm humid climate changed to dry and hot seasonal conditions, thus the terrestrial sedimentation of some river-delta-lake facies in the southern edge of the Junggar Basin were affected by the climate changes, resulting in the overall shallowing of the water system and the increasing salinity to form a sedimentary environment dominated by saline lacustrine background (Lou et al., 2022). In this tectonic-sedimentary context, the Middle Permian Jingjingzigou Formation is characterized by the widespread development of tuffs or tuffaceous intercalations or lenses, and the lithology is mainly purple-red siltstone or sandy mudstone interspersed with gray-white tuffs or tuffaceous mudstone.

3 Sampling and methods

3.1 Samples

The samples for this study are selected from the cores and field outcrops of the Upper Triassic Yanchang Formation in the Ordos Basin (Figure 1) and the Middle Permian Jingjingzigou Formation in the southern margin of the Junggar Basin (Figure 2).

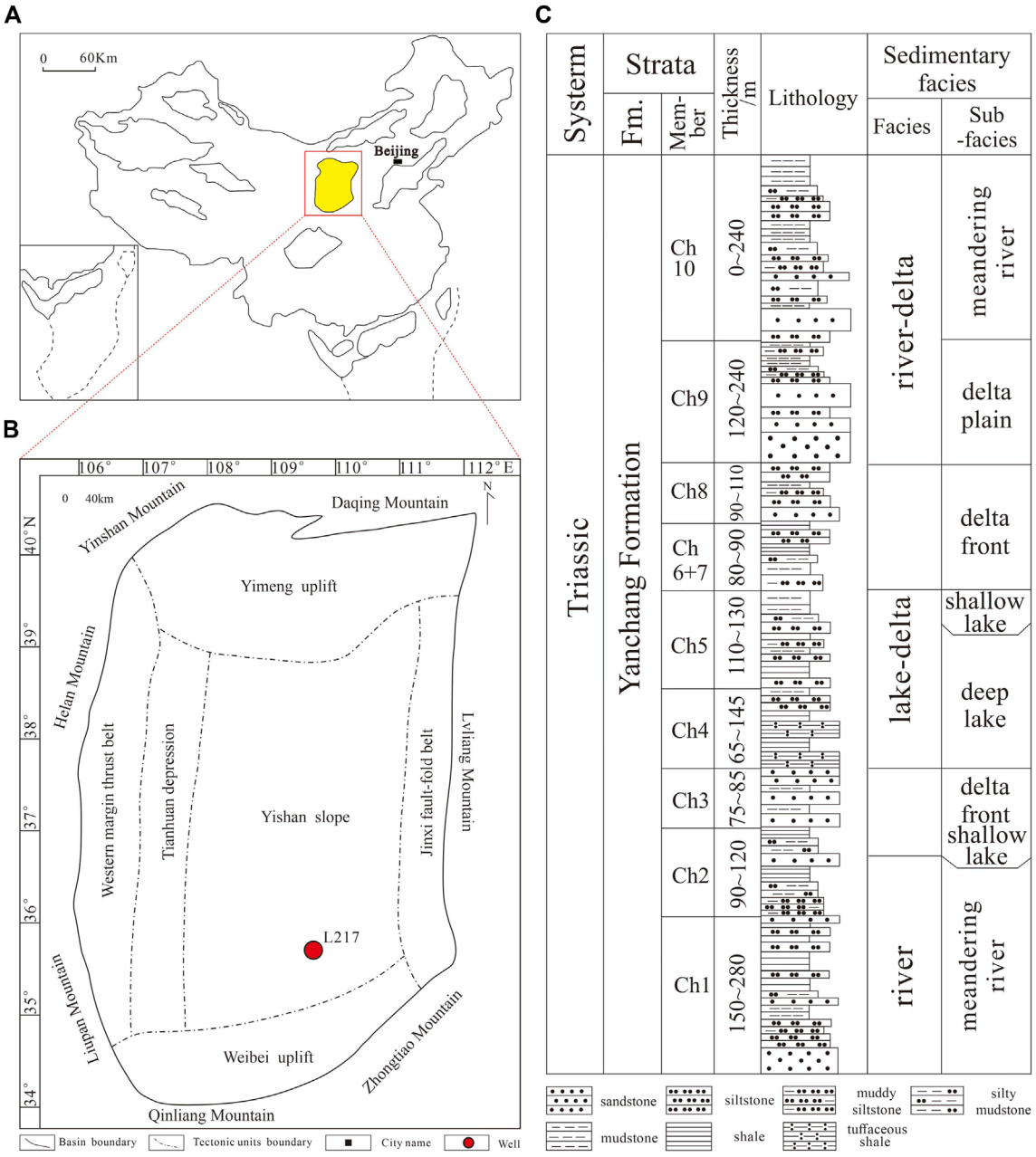

FIGURE 1
(A) Geographic location of the Ordos Basin in China; **(B)** geological background of the Ordos Basin, as well as the study area and well location; **(C)** stratigraphy, thickness, lithology, and sedimentary phases of the Upper Triassic Yanchang Formation in the Ordos Basin.

In addition, the samples required for the experiment are described below and prepared according to different experimental requirements.

3.2 Methods

3.2.1 X-ray diffraction (XRD) analysis

The *XRD* analysis is a research tool that performs on a material, analyzing its diffraction pattern and obtaining information such as the composition of the material, the structure or morphology of the atoms or molecules inside the material. As a main method to study the physical phase and crystal structure of substances, the XRD analysis of power less than 200 mesh (i.e., <75 mm) were performed at Craton Technology Co., Ltd., Beijing, China. The measurements were conducted on a Bruker D8 DISCOVER diffractometer with Co. Kα-radiation at 45 Kv and 35 mA, following the two independent processes of the CPSC procedure. The diffracted beam was measured foreach step of 0.02° 2θ via a scintillation detector with counting time of 20 s, and diffractograms were obtained from 2° to 76°

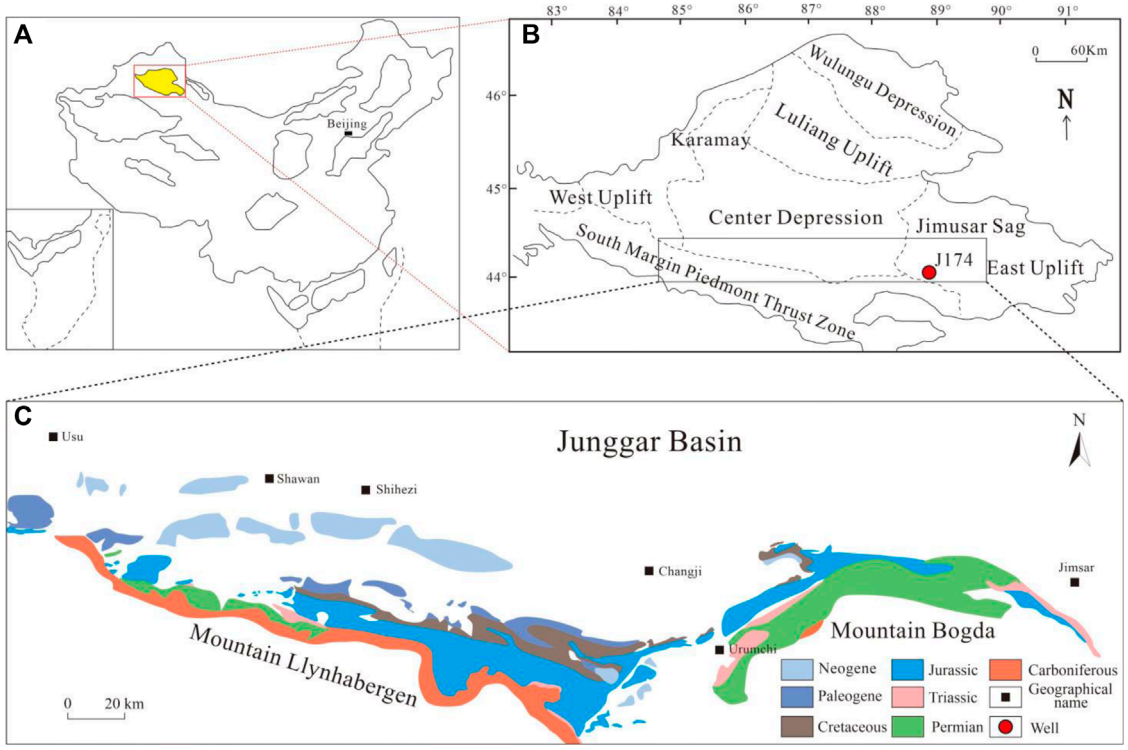

FIGURE 2
(A) Geographical position of the Junggar Basin in China; **(B)** tectonic position of the southern margin of E Junggar Basin, as well as the study area and well location; **(C)** geological map of the southern margin of the Junggar Basin.

2θ. A total of 26 tuffaceous shale samples from the Jingjingzigou Formation and Lucaogou Formation of Middle Permian in Junggar Basin, and from the Yanchang Formation of Upper Triassic in Ordos Basin were measured using whole rock X-ray diffraction experiments. Quantitative phase analysis was conducted using Rietveld refinement.

3.2.2 FE-SEM observation

The ultra-high resolution FE-SEM can do secondary electron image and reflection electron image observation and image processing of various solid sample surface morphology. Combined with the high-performance X-ray spectrometer, it can simultaneously perform qualitative, semi-quantitative and quantitative analysis of the micro-area point-line elements of the sample surface and has the ability of comprehensive analysis of morphology and chemical components (Li et al., 2020; Gao et al., 2021). The most important feature of field emission scanning electron microscopy instrument is that it has ultra-high-resolution scanning image observation ability, especially the use of the latest digital image processing technology, providing high-power, high-resolution scanning images, is the most effective instrument for nanomaterials particle size testing and surface morphology observation of micron and nanoscale samples, and is more and more widely used in geological leaders (Chen and Xie, 2005; Gu and Li, 2020). Six samples from different layers of tuffaceous shale in Jingjingzigou Formation and Lucaogou Formation of Middle Permian in Junggar Basin and Yanchang Formation of Upper Triassic in Ordos Basin were tested by FE-SEM (FEI HELIOS NANOLAB 650 SEM) at the National Key Laboratory of Petroleum Resources and Engineering, China University of Petroleum (Beijing), and a detailed description of the technical procedure is given in the Chinese Oil and Gas Industry Standards (SY/T5162-1997).

3.2.3 Contact angle measurements

The contact angle is the angle between the tangent line made to the surface of the droplet and the solid-liquid surface when the liquid is stabilized by contact with the solid, after passing through the intersection of gas, liquid and solid phases. When dropping droplets on a solid plane at constant temperature and pressure, the droplets can automatically spread out on the solid surface or at an angle to the solid surface. There are many measurement methods to measure the contact angle, such as the suspension droplet method, tension measurement method, tilting plate method, Washburn method, and so on. The more commonly used method for measuring the contact angle of oil and gas reservoirs is the suspension droplet method. The suspension drop method is simple and easy to operate, with short testing time. However, the heterogeneity of the rock has a greater impact on it. Especially, unconventional reservoir mineral composition is complex and unevenly distributed, with heterogeneity of rocks. Based on the heterogeneous characteristics of the rock surface, the measurement angle varies widely, thus the method of averaging is generally utilized to represent the rock surface wettability. This study mainly used

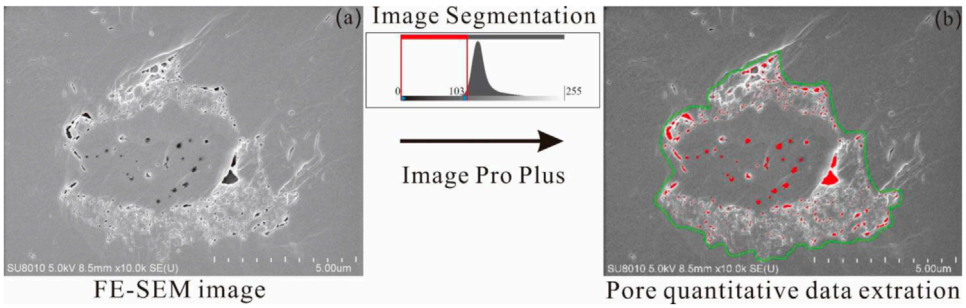

FIGURE 3
Pore extraction software process. **(A)** Original images under scanning electron microscopy; **(B)** scanning electron microscopy images extracted and quantitatively processed through IPP.

the German KRUSS DSA30S droplet analyzer to determine the contact angle between the solution and the sample surface. The instrument is equipped with a high-speed camera with a high-precision lens, which can record the dynamic spreading movement of different titration liquids on the shale surface through the high-speed camera, obtain a digital image of the shale surface, and realize semi-automatic retrieval of the droplet shape, determination and calculation of the contact angle through the system software. Seven samples of tuffaceous shale from Lucaogou Formation in Ordos Basin and Jingzigou Formation of Middle Permian in the Junggar Basin were measured for contact angle. Three samples from Well Lu217 in Ordos Basin were recorded as Lu217-1, Lu217-2 and Lu217-3; Four samples in the Junggar Basin, one from JJZG-04F well, one from JJZG-05F well, and two from JJZG-08F well, recorded as JJZG-08F-1 and JJZG-08F-2; And analyze the experimental results.

3.2.4 Spontaneous imbibition measurements

Spontaneous imbibition is a common natural phenomenon occurring in porous media rocks. When porous media rocks and wetting liquids are in contact, the rocks will spontaneously draw in the wetting liquid under the action of capillary forces. Spontaneous imbibition is mainly dependent on the pore structure of porous media, capillary forces and rock-fluid interactions. Therefore, the pore connectivity and wettability of shale can be reflected by using spontaneous imbibition experiments. The more hydrophilic the rock is, the greater the capillary force and the faster the spontaneous imbibition rate, otherwise, the slower the rate. The spontaneous imbibition experimental apparatus includes electronic analytical balance, timer, hook, core holder, glass tray, adjustable elevator, computer, and so on. The experimental equipment is placed in a constant temperature and humidity environment to reduce the influence of liquid evaporation as well as air flow on the core self-imbibition experiment. Spontaneous imbibition experiments were carried out on four tuffaceous shale samples from the Lucaogou Formation in the Ordos Basin and the Jingzigou Formation in the Middle Permian in the Junggar Basin. Among them, two samples from well Lu217 in the Ordos Basin are Lu217-1 and Lu217-2, and two samples in the Junggar Basin, one from well JJZG-05F and one from well JJZG-08F; And analyze the experimental results.

3.3 Data processing methods

3.3.1 Plane porosity calculations

Using Image Pro Plus (IPP) software to statistically analyze the images captured by FE-SEM observation, the software can identify various pores and obtain the basic parameters of pore characteristics, such as area, perimeter, pore diameter, and so on. The software is able to identify the pores by using the grayscale value of each pixel in the image, combined with manual recognition and statistics to determine reasonable thresholds, thus accurately determining the basic parameters of the microscopic pores of the sample. The extraction of quantitative pore data by IPP image processing software can be divided into the following three steps (Figure 3): ① image reference scale setting; ② sample SEM image pore identification; ③ pore quantitative data extraction.

3.3.2 Wettability parameter calculation

The contact angle has been used as the most intuitive and effective method to evaluate the interfacial wettability. The degree of rock-fluid wettability has been classified using the angles of deionized water and n-decane when they are in contact with the sample surface: water wettability when the contact angle $\theta < 75°$; neutral wettability when $105° > \theta > 75°$; and oil wettability when $\theta > 105°$ (Wang et al., 2012), combining with previous work using contact angle to calculate wettability parameters to establish a set of wettability parameter discriminatory criteria (Gao et al., 2022). The contact angle wettability parameter calculation equation is as follows:

$$\mathrm{CAI} = \frac{90 - \theta_w}{90} - \frac{90 - \theta_O}{90} \quad (1)$$

where: CAI (Contact Angle Index) is the contact angle wettability parameter, θ_w is the water wettability angle, and θ_o is the oil wettability angle.

4 Results

4.1 Mineralogical characteristics

According to the whole-rock XRD analysis, it is worth noting that there are characteristic minerals/mineral assemblages

10.3389/feart.2024.1410585

TABLE 1 Mineralogical composition (XRD) in tuffaceous shales of Upper Triassic Yanchang Formation and Middle Permian Jingjingzigou Foumation.

Sample HD	Mineral content %										
	Clay mineral	Quartz	K-feldspar	Plagioclase	Calcite	Dolomite	Ankerite	Anhydrite	Siderite	Pyrite	Barite
Lu217-2	64.3	4.9	—	2.5	—	28.2	—	—	—	—	—
Lu217-1	84.7	8.9	2.9	3.1	—	—	—	—	0.4	—	—
JJZG-08F	—	4	—	17.5	—	—	71.5	—	—	—	6.9
JJZG-05	9.7	9.7	—	28	14.9	—	21.6	4.8	1.5	9.6	—
JJZG-04F	18	3.9	—	20.1	—	—	50.5	—	—	—	7.5

composed of ankerite (average of 47.9 wt.%), anhydrite (average of 4.8 wt.%) and pyrite (average 9.6 wt.%) occurring in the tuffaceous shales of the Middle Permian Jingjingzigou Formation, suggesting that development of saline lacustrine basin as a result of intense input of (sedimentary) tuff can significantly enhance the reducibility of lacustrine water body (Jiang, 2019; Wang et al., 2023). Additionally, tuffaceous shales of the Upper Triassic Yanchang Formation yield an obviously higher average concentration of clay minerals around 74.5%, implying a substantial difference exist in terrigenous provenance composition between the fresh-water and saline fine-grained mixed sedimentary sequences. Quantification of all the analyzed minerals are listed and illustrated in Table 1 and Figure 4.

4.2 Pore types

A complex pore system composed of large amount of primary and secondary pores are observed and confirmed using FE-SEM in the targeted tuffaceous shale reservoirs, including devitrified intergranular-intercrystalline pores, dissolution pores, organic matter related pores, as well as microfractures. This is interpreted as a result of devitrification processes during the diagenesis. The detailed characteristics of the main identified pore categories are summarized as follows, respectively.

4.2.1 Intergranular-intercrystalline pores

A large amount of intergranular-intercrystalline pores are observed by using FE-SEM analysis as clastic/authigenic in origin (Figures 5A–D), and the secondary intergranular-intercrystalline pores are mostly speculated to be formed as a result of devitrification triggering the transformation of unstable vitreous constituents into siliceous pyroclasts, silicate components and even microcrystals (Mchenry, 2009; Kirov et al., 2011), which facilitates a significant reduction in rock volume and increase in secondary porosity of the tuffaceous shale reservoirs (Ma et al., 2015). Additionally, from the perspective of polygonal/irregular morphology and randomly distributed patterns, the distribution of observed intergranular-intercrystalline pores are considered to be conducive to the improvement in pore connectivity, and the formation and development of pore systems. To sum up, concerning the differential development of intergranular-intercrystalline pores observed in the Upper Triassic Yanchang Formation tuffaceous shales (Figures 5A, B) and the Middle Permian Jingjingzigou Formation tuffaceous shales (Figures 5C, D), it is concluded that the intergranular-intercrystalline pores of the tuffaceous shales prevailing in the saline lacustrine settings were better developed.

4.2.2 Dissolution pores

Dissolution pores are also widely distributed in siliceous and feldspar particles of tuffaceous shales as evidenced by FE-SEM observation, characterized by an irregular morphology (e.g., subcircular, curved and crescent shaped) with dissolved edges, and wide range in pore size (Figures 5C, E–G). In fact, devitrification and dissolution processes are the most important synchronous interactions during the diagenesis of tuffaceous shale reservoirs. Compared to the tuffaceous shale of the Upper Triassic Yanchang Formation (Figure 5E), the tuffaceous shale of the Middle Permian

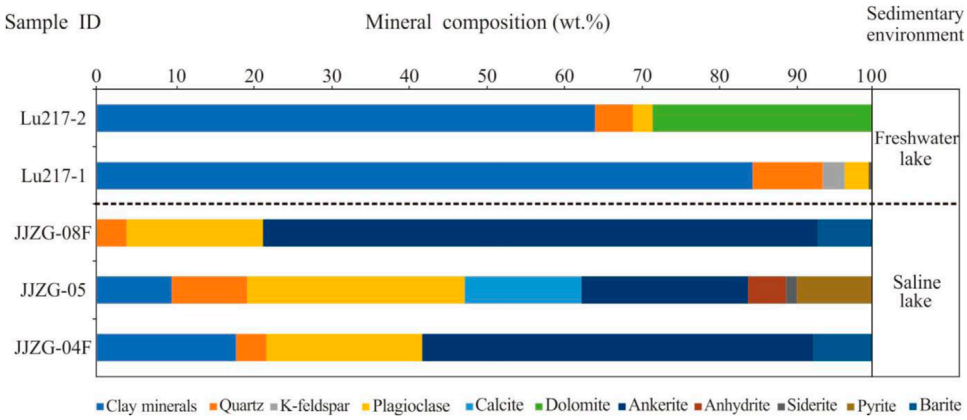

FIGURE 4
Whole-rock mineral composition in tuffaceous shales of the Upper Triassic Yanchang Formation and Middle Permian Jingjingzigou Formation.

Jingjingzigou Formation (Figures 5F–G) has better developed dissolution pores.

4.2.3 Microfractures

Numerous microfractures are also observed and mostly well-developed along the boundary between organic matter and inorganic particles/the bedding planes and bitumen pores elongated between similarly oriented clay sheets, or appear obliquely across the organic matter laminations and inorganic matrixes (Figures 5H–J). These observed microfractures contribute significantly to interconnected reservoir spaces and also the seepage capacity of tuffaceous shales by forming pore-microfracture networks, and are typically interpreted to be associated with tectonism, dehydration, dry shrinkages, mineral recrystallization, as well as hydrocarbon generation during burial and diagenesis processes (Marquez and Mountjoy, 1996; Nan et al., 2007; Wang and Sun, 2009; Yao and Liu, 2009; Zhao et al., 2009; Zhang et al., 2021). Compared to the tuffaceous shale of the Middle Permian Jingjingzigou Formation (Figure 5J), the microfractures in the tuffaceous shale of the Upper Triassic Yanchang Formation appears less developed (Figures 5H, I).

4.2.4 Organic matter related pores

Compared to those of typical marine shale reservoirs such as the Lower Silurian Longmaxi shales of Southwest China, organic matter related pores in lacustrine shale reservoirs appear to be less developed (Mastalerz et al., 2013; Guan et al., 2016). Concerning the significant impact of thermal maturity on development of organic matter pores, the effective organic matter pore spaces are generally not developed in the studied low-mature tuffaceous shales characterized by vitrinite reflectance (R_o) lower than 0.8% (Wang and Guo, 2019; Wang et al., 2023). That is to say the relatively low maturity can restrict the development of organic matter pores in tuffaceous shales.

However, shrinkage and bitumen-hosted pores are relatively developed and locally orientated parallel/sub-parallel to argillaceous bedding planes, or occurs along the edges of brittle mineral grains positioned adjacent to the margins of solid bitumen residues/primary organic matter particles (Figures 5K, L) (Wang and Sun, 2009; Wood et al., 2015; Camp, 2017). It is worth noting that these organic matter related pores occurring along the grain margins, identified as the main prevailing type always yield the width less than 1 μm.

4.3 Spontaneous imbibition behavior

Spontaneous imbibition experiments of water and oil imbibition (n-decane) are performed on the selected samples from two basins in Table 2. In the experiment, there is a period of instability of about 1 min at the beginning, which is related to the open pore connectivity and wettability of the sample surface. After the instability period, a clear linear relation between the logarithm of the cumulative height of imbibition and the logarithm of the imbibition time of the samples is observed in the plot (Figure 6). The slope value of spontaneous imbibition can reflect the pore connectivity of the samples.

The experimental results show that the spontaneous imbibition slopes of deionized water and n-decane for the Upper Triassic Yanchang Formation samples range from 0.310 to 0.330 with an average of 0.320, and from 0.392 to 0.440 with an average of 0.416, respectively (Figures 6a,b, a',b'), while the spontaneous imbibition slopes of deionized water and n-decane for the Middle Permian Jingjingzigou Formation samples range from 0.359 to 0.366 with an average of 0.363, and from 0.460 to 0.500 with an average of 0.480, respectively (Figures 6c,d, c',d') (Table 2). Thus, the tuffaceous shales developed in saline lacustrine settings yields obviously higher imbibition slopes, indicating a better pore-microfracture connectivity than that of fresh-water sedimentary environments.

4.4 Wettability characteristics

The contact angles of deionized water and n-decane of Upper Triassic Yanchang Formation samples and Middle Permian Jingjingzigou Formation samples are obtained by the contact angle measurement experiments. The experimental results show that the deionized water and n-decane contact angles of the Upper

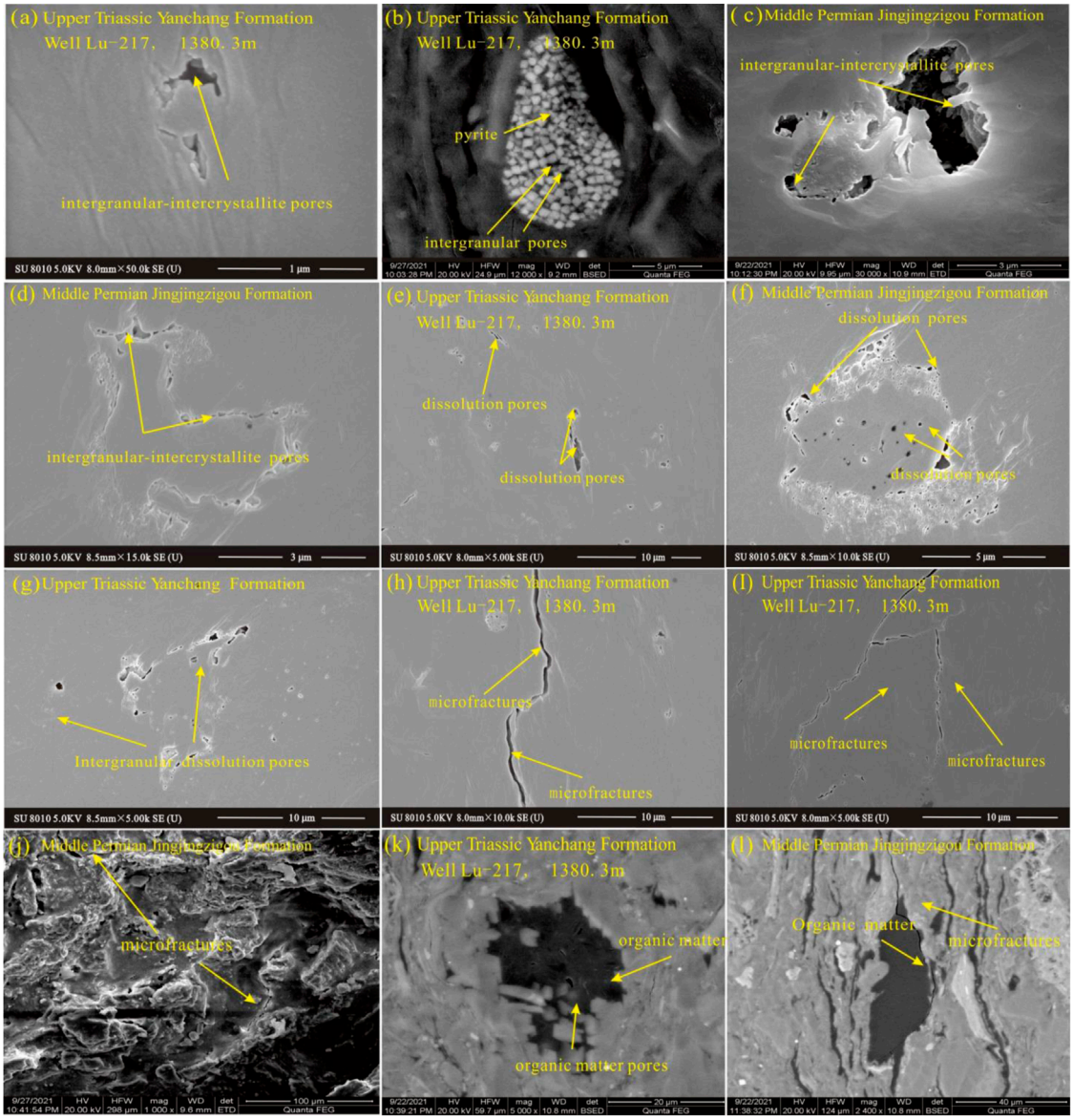

FIGURE 5
FE-SEM images of tuffaceous shale samples from the Upper Triassic Yanchang Formation **(A–F)** and Middle Permian Jingjingzigou Formation **(G–L)**. **(A)** Typical intergranular-intercrystalline pore features (few isolated devitrified pores, but signs of crystallite); **(B)** development of pyrite and intergranular pores; **(C)** typical dissolution pores; **(D)** microfracture characteristics with a few dissolved pores; **(E)** typical grain-edge microfracture characteristics (microscopic stylolites); **(F)** organic matter pores; **(G)** typical intergranular-intercrystalline pore with recrystallization; **(H)** typical intergranular-intercrystalline pore pores and peripheral devitrified pores (with crystallite); **(I)** dissolution pores (with crystallite phenomenon); **(J)** dissolution pore; **(K)** microfracture characteristics; **(L)** organic matter filled in microfractures.

TABLE 2 Experimental results of spontaneous imbibition of tuffaceous shale samples from the Upper Triassic Yanchang Formation and Middle Permian Jingjingzigou Formation.

Sample ID	Spontaneous imbibitions (deionized water) slope	Spontaneous imbibitions (n-decane) slope
Lu217-1	0.330	0.392
Lu217-2	0.310	0.440
JJZG-05F	0.366	0.460
JJZG-08F	0.359	0.500

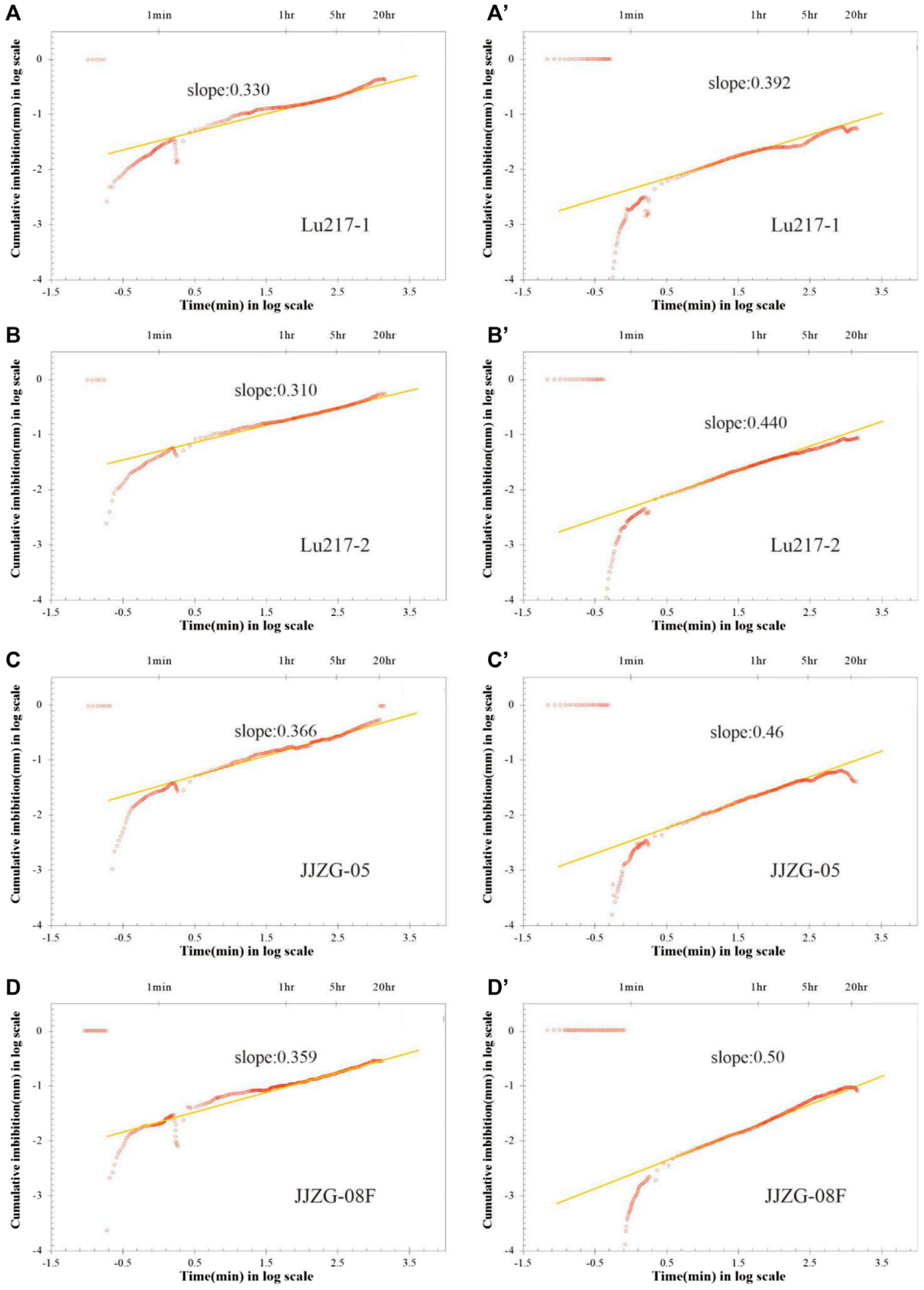

FIGURE 6
Spontaneous imbibition results of tuff aceous shale samples from the Upper Triassic Yanchang Formation and Middle Permian Jingjingzigou Formation. **(A–D)** Images of spontaneous imbibition results of deionized water from tuff aceous shale samples of the Upper Triassic Yanchang and Middle Permian Jingjingzigou Formations; **(A'–D')** Images of spontaneous imbibition results of n-decane from tuff aceous shale samples of the Upper Triassic Yanchang and Middle Permian Jingjingzigou Formations.

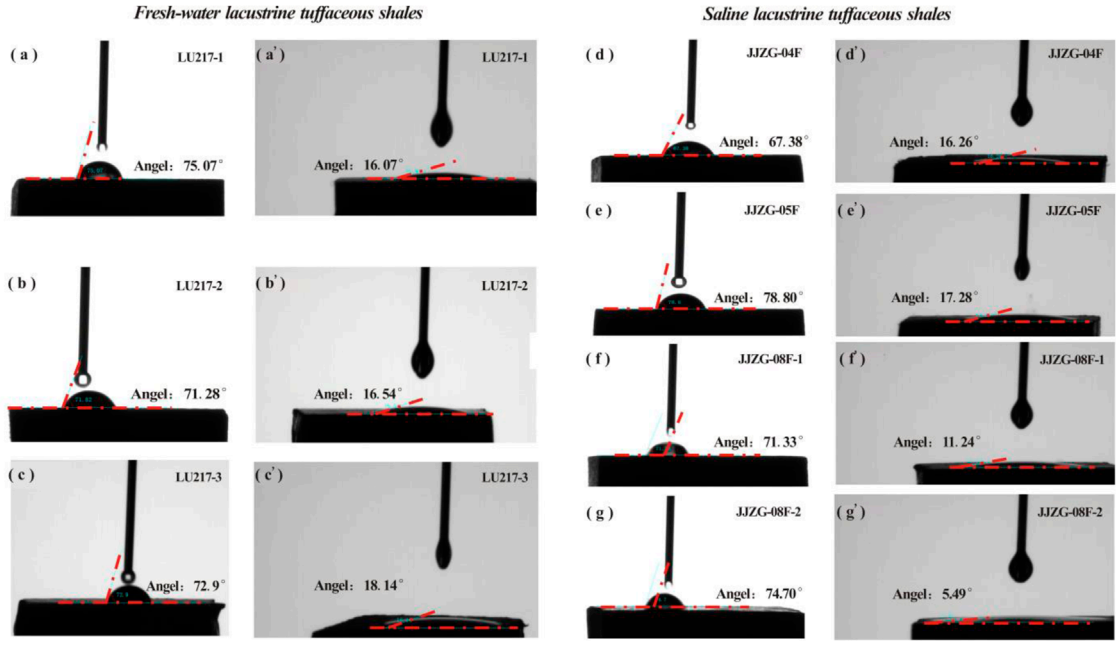

FIGURE 7
Determination of wettability angle of tuffaceous shale samples from the Upper Triassic Yanchang Formation and Middle Permian Jingjingzigou Formation. **(A–C)** Images of deionized water contact angle results of tuffaceous shale samples from the Upper Triassic Yanchang Formation; **(D–G)** images of deionized water contact angle results of tuffaceous shale samples from the Middle Permian Jingjingzigou Formation; **(A′–C′)** images of n-decane contact angle results of tuffaceous shale samples from the Upper Triassic Yanchang Formation; **(D′–G′)** images of n-decane contact angle results of tuffaceous shale samples from the Middle Permian Jingjingzigou Formation.

TABLE 3 Wettability parameters calculation method and assessment criteria.

Measurement methods	Measurement parameters and calculation methods	Assessment criteria		
		Water wetting	Neutrally wetting	Oil wetting
Contact angles	θ	$\theta \leq 75°$	$75° < \theta < 105°$	$\theta > 105°$
CAI	$CAI = (\theta_o - \theta_w)/90$	$CAI \geq -0.67$	$-1 < CAI < -0.67$	$CAI \leq -1$

Triassic Yanchang Formation tuffaceous shales range from 71.82° to 75.07° with an average of 73.26°, and from 16.07° to 18.14° with an average of 16.92°, respectively, while the deionized water and n-decane contact angles of the Middle Permian Jingjingzigou Formation tuffaceous shales range from 67.38° to 78.80° with an average of 73.05°, and from 5.49° to 17.28° with an average of 12.57°, respectively (Figure 7; Tables 3, 4). Thus, according to the wettability evaluation criteria, the targeted tuffaceous shale developed in the saline lacustrine settings tends to be more oil-wet than that of fresh-water lacustrine sedimentary environments.

Additionally, the Contact Angle Index (CAI) inferred by recent publications are used here as an important proxy for determining tuffaceous shale wettability as described by the above calculation Equation 1. The calculated CAI indicators of the Upper Triassic Yanchang Formation and Middle Permian Jingjingzigou Formation range from −0.66 to −0.61 with an average of −0.63, and from −0.77 to −0.57, with an average of −0.67, respectively (Table 3, 4). These evaluation results clearly suggest that tuffaceous shales developed in the saline lacustrine settings are characterized by more oil-wet wettability, i.e., an oleophilic surface, compared to those of fresh-water lacustrine settings (Figure 8).

5 Discussion

5.1 Mechanism for differentiation of fresh-water and saline water devitrification degree

Volcanic clastic material is a sediment with a mixture of plastic, rigid and semi-plastic particles, mainly composed of microscopic vitric fragments, crystal fragments (feldspar, quartz, and so on) and rock fragments in an aggregate dominated by aluminosilicate minerals, containing small amounts of clay minerals and pyrite (Wang et al., 2005; Zhu et al., 2014). Since the vitreous thermodynamic properties of volcanic clastic materials are very

TABLE 4 Contact angle and wettability parameters of tuffaceous shale samples from the Upper Triassic Yanchang Formation and Middle Permian Jingjingzigou Formation.

Sample ID	Water contact angle (θ_w/°)	Average water contact angle	Oil contact angle (θ_w/°)	Average oil contact angle	Wettability parameters (CAI)	Average wettability parameters	Wettability
Lu-217-1	75.07		16.07		−0.66		Hydrophilic
Lu-217-2	71.82	73.26	16.54	16.92	−0.61	−0.63	Hydrophilic
Lu-217-3	72.9		18.14		−0.60		Hydrophilic
JJZG-04F	67.38		16.26		−0.57		Hydrophilic
JJZG-05F	78.8	73.1	17.28	12.57	−0.68	−0.67	Oleophilic
JJZG-08F-1	71.33		11.24		−0.67		Oleophilic
JJZG-08F-2	74.7		5.49		−0.77		Oleophilic

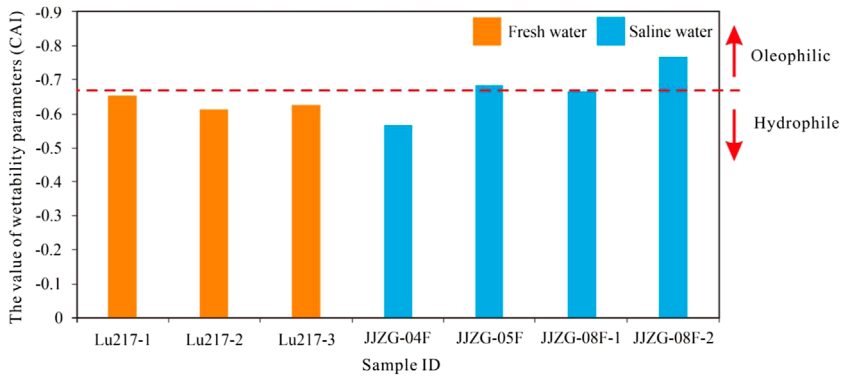

FIGURE 8
Difference in the wettability parameters of tuffaceous shales from fresh-water and saline lacustrine environments.

instable, vitreous components such as vitric fragments can be easily converted into crystals, namely, devitrification (Marshall, 1961). During the burial process, with the change of environmental conditions such as temperature, pressure and fluid properties, the devitrification and dissolution carried out within the volcanic clastic materials are affected to different devitrification degrees, which are mainly reflected in the crystallization, dissolution and reprecipitation of volcanic materials and the migration and transformation of ions. In the process of migration and conversion, some components of the volcanic clastic materials migrate out of the local system with the formation water, while the remaining components crystallize or precipitate to form new crystallite or microcrystalline authigenic minerals, meanwhile the overall volume of the tuff decreases and a large number of pores are formed, meaning devitrification pores. Devitrification pores are usually micro-nanometer pores, as well as a large number of pores and good connectivity within a highly devitrified reservoir, which can be used as an important storage space in tuffaceous reservoirs (Zheng et al., 2018b). Microcrystalline quartz formed by devitrification can be observed under SEM, with a large number of intercrystalline pores formed between these microcrystalline quartz particles, capable of serving as an effective storage space for oil and gas. Devitrification is influenced by many factors, such as temperature, pressure, organic acids, and formation water action. During diagenesis, with the increase of temperature and pressure, the activity and rearrangement rate of thermodynamically unstable vitreous internal masses in tuff reservoirs are accelerated, which is favorable for the positive proceeding of devitrification and conversion to crystals, such as microcrystalline quartz, feldspar and zeolite (Ma et al., 2015).

The degree of devitrification is significantly affected by the action of organic acids, during devitrification many silicate minerals are produced, which will be dissolved by complexation with organic acids under acidic conditions and carried away by pore fluids, shifting the chemical equilibrium of the whole devitrification to the positive reaction direction and promoting devitrification. The dynamic process of volcanic material and formation water has an important influence on the devitrification process of volcanic material. Alkaline formation water can cause the dissolution of quartz and accelerate the reduction of Si in the reservoir, which makes volcanic vitreous dissolve and

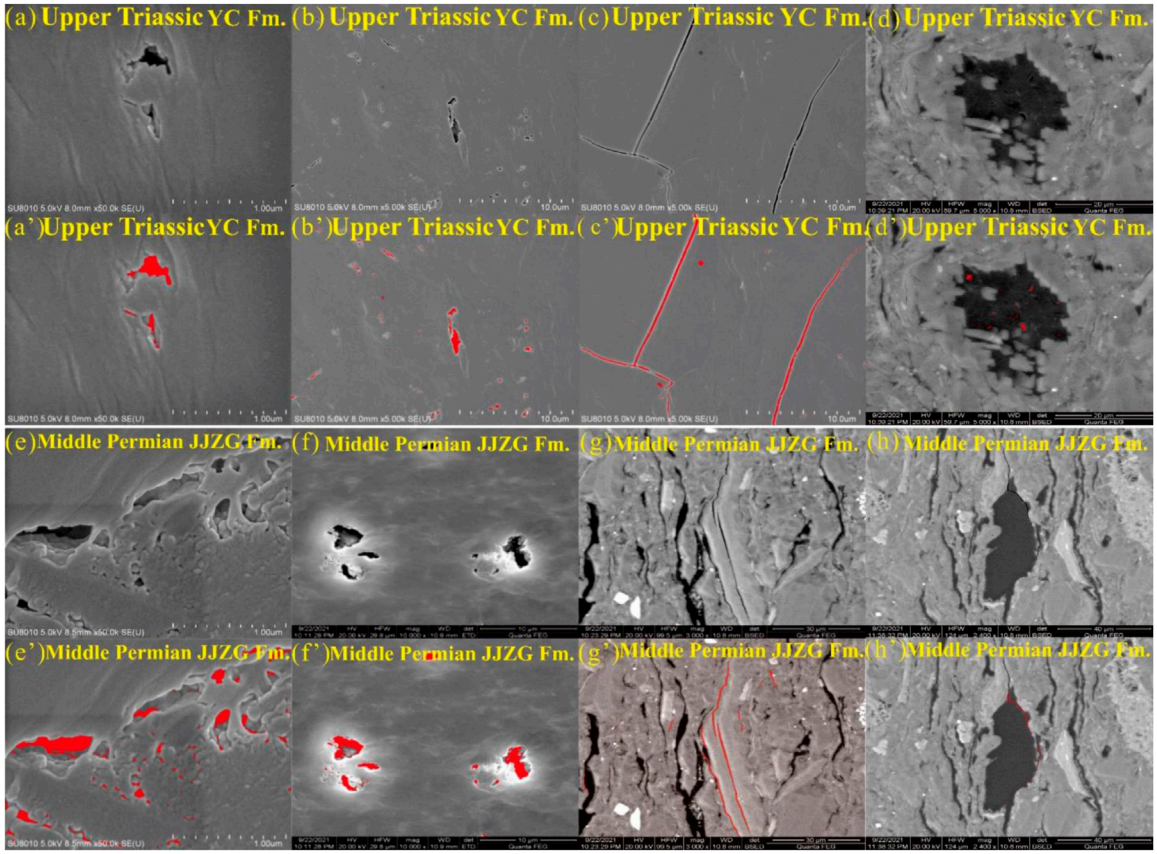

FIGURE 9
Porosity extraction of tuffaceous shales pore surfaces of the Upper Triassic Yanchang Formation and Middle Permian Jingjingzigou Formation. **(a–h)** Original FE-SEM images showing the characteristics of observed pores and micro-fractures; **(a'–h')** Extraction of targeted pores and micro-fractures from the investigated FE-SEM images.

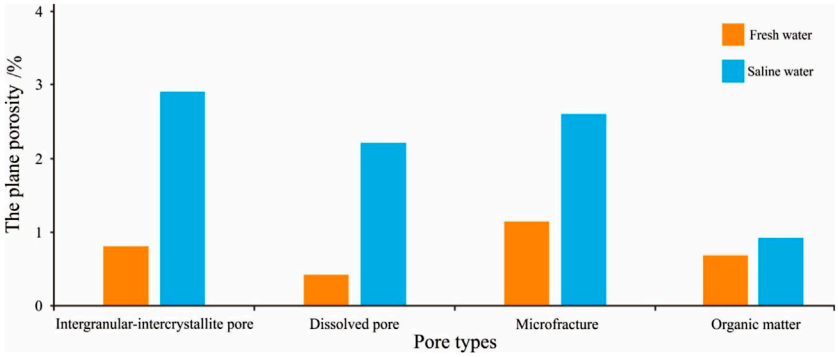

FIGURE 10
Difference in plane porosity of tuffaceous shale samples in fresh-water and saline lacustrine environments.

devitrification (Qiu et al., 2002) and form a large number of authigenic minerals with other metal ions, such as K-feldspar, zeolite, montmorillonite, illite, chlorite, and so on (Zhu et al., 2014). With the continuous precipitation of alkali metal ions such as Na, K, Ca, Mg, Fe, the volcanic materials contain only Si and O, and finally crystallize to form authigenic quartz, which can promote the devitrification process.

According to XRD analysis, carbonate minerals occupy a high proportion (36.5 wt.%–71.5 wt.%, average 52.8 wt.%) in tuffaceous shale samples of the Middle Permian Jingjingzigou Formation, moreover, the carbonate mineral composition is mainly ankerite. Following the International Mineralogical Association guidelines (Nickel and Grice, 1998) when Fe replaces more than half of the Mg in the dolomite lattice, it is called ankerite. As a kind

of dolomite, the formation environment of iron dolomite is similar to that of dolomite, which is a saline environment with high water salinity and high pH.

Based on previous studies, it is shown that the paleoclimate was warm and humid during the deposition of the Upper Triassic Yanchang Formation in the Ordos Basin, with the water bodies forming a fresh-water environment (Fu et al., 2009), furthermore, the tuff rich Chang seven member was formed at the peak of lake basin development and the most extensive lake area in the whole basin (Fu et al., 2020). However, the depositional period of the Jingjingzigou Formation on the southern margin of the Junggar Basin changed from a wet paleoclimate to a seasonal dry and hot climate, and some terrestrial deposits in the fluvial-delta-lacustrine facies were affected by the climate shift resulting in an overall shallowing of the water column and an increase in water salinity to form a saline lake basin background dominated by sedimentary environment (Lou et al., 2022). Therefore, in a significantly different depositional context, the samples of the Upper Triassic Yanchang Formation and the samples of the Middle Permian Jingjingzigou Formation are subject to significant differences in devitrification, in addition, the pore structure characteristics and wettability of the samples from the two regions are significantly different under the influence of the degree of devitrification.

The devitrification effect is obvious for the transformation of the pore-forming matrix. The IPP technique is used to extract the three types of intergranular-intercrystalline, dissolved pores and microfractures in the SEM photographs of each sample and calculate the corresponding plane porosity (Figure 9). Using the plane porosity to reflect the degree of pore development within the reservoir under the influence of devitrification. The results show (Figure 10) that the maximum plane porosity of intergranular-intercrystalline pore of the Upper Triassic Yanchang Formation samples can reach 0.81%, the maximum plane porosity of dissolved pore can reach 0.43% and the maximum plane porosity of microfracture can reach 1.14%, respectively, and the pore development of devitrified degree of samples is not well developed and the devitrified effect is weak. Under the same field of vision, the sample of the Middle Permian Jingjingzigou Formation has a maximum of 2.91% of intergranular-intercrystalline pore plane porosity, 2.21% of dissolved pore plane porosity and 2.60% of microfracture plane porosity. The samples have well-developed devitrified pores and are obviously subject to devitrified effect. The comparison of the porosity of three types of these samples, including intergranular-intercrystalline pores, dissolved pores and microfractures, in the two regions shows that the pore development of the Middle Permian Jingjingzigou Formation samples is better, with a higher degree of devitrification. After devitrification, plastic vitric pyroclastic in tuff is converted into microcrystalline quartz and feldspar. Quartz and feldspar particles have good compaction resistance and can prevent pores from being destroyed by compaction so as to provide good support in shale reservoirs. The content of quartz-feldspathic in samples from the Middle Permian Jingjingzigou Formation (21.5 wt.% – 37.8 wt.%; average 27.8 wt.%) is greater than that of quartz-feldspathic in samples from the Upper Triassic Yanchang Formation (7.4 wt.% – 14.8 wt.%; average 11.2 wt.%), indicating that the mineral skeleton of the samples of the Middle Permian Jingjingzigou Formation is more well supported and provides good protection for the pore space. The above two factors together are important reasons for the degree of devitrification to control the pore development and pore preservation ability of tuffaceous reservoirs.

5.2 Control of pore structure characteristics and interfacial wetting effects by differential devitrification

The samples of the Middle Permian Jingjingzigou Formation are subject to a higher degree of devitrified action than those of the Upper Triassic Yanchang Formation. The spontaneous imbibition experiments show that the spontaneous imbibition slope of deionized water (0.366 ~ 0.359) and the spontaneous imbibition slope of n-decane (0.460 ~ 0.500) of the Middle Permian Jingjingzigou Formation samples are greater than the spontaneous imbibition slope of deionized water (0.310 ~ 0.330) and the spontaneous imbibition slope of n-decane (0.392 ~ 0.440) of the Upper Triassic Yancheng Formation samples. This shows that the pore connectivity of the Middle Permian Jingjingzigou Formation tuffaceous shales is better than that of the Upper Triassic Yanchang Formation tuffaceous shales. The higher spontaneous imbibition slope of the sample from the Middle Permian Jingjingzigou Formation indicates that the tuff-bearing reservoir has a higher degree of devitrification and better pore connectivity. After devitrification, a large number of intergranular pores and dissolution-associated pores are formed in the Middle Permian Jingjingzigou Formation tuffaceous shales, forming an effective pore network under the communication effect of microfractures, which serves as a imbibition channel for formation fluids and organic fluids and also provides fluid exchange space for tuff dissolution, accelerating the process of devitrification and dissolution around the microfractures and positively promoting the formation of effective pores and the connectivity between various pores. In contrast, the devitrification of tuffaceous shales of the Upper Triassic Yanchang Formation is weak, the development of devitrification pores in the reservoir is limited, making it difficult to form an effective pore network, so that the effective imbibition channels of geological and organic fluids are difficult to form, which reduces the process of devitrification and dissolution of tuff and makes the pore connectivity in the reservoir lower. Therefore, the pore connectivity of the Middle Permian Jingjingzigou Formation tuffaceous shales is better than that of the Upper Triassic Yanchang Formation tuffaceous shales.

According to the spontaneous imbibition experiment, it is concluded that the spontaneous imbibition slope of n-decane is greater than the spontaneous imbibition slope of deionized water for the tuffaceous shales of the Middle Permian Jingjingzigou Formation and the tuffaceous shales of the Upper Triassic Yanchang Formation (Figure 11), besides, the difference between the spontaneous imbibition slope of deionized water (0.366 ~ 0.359) and the spontaneous imbibition slope of n-decane (0.460 ~ 0.500) is greater in the tuffs of the Middle Permian Jingjingzigou Formation. It indicates that the interfacial wettability within the tuff reservoir has been changed after devitrification, moreover, the difference in the degree of devitrification affects the degree of change of interfacial wettability within the reservoir. The degree of devitrification of tuffaceous shales in the Middle Permian Jingjingzigou Formation is obvious. When the tuff components in the reservoir are devitrified, the hydrophilic substances such as vitreous matter are reduced, which changes the wetting at the

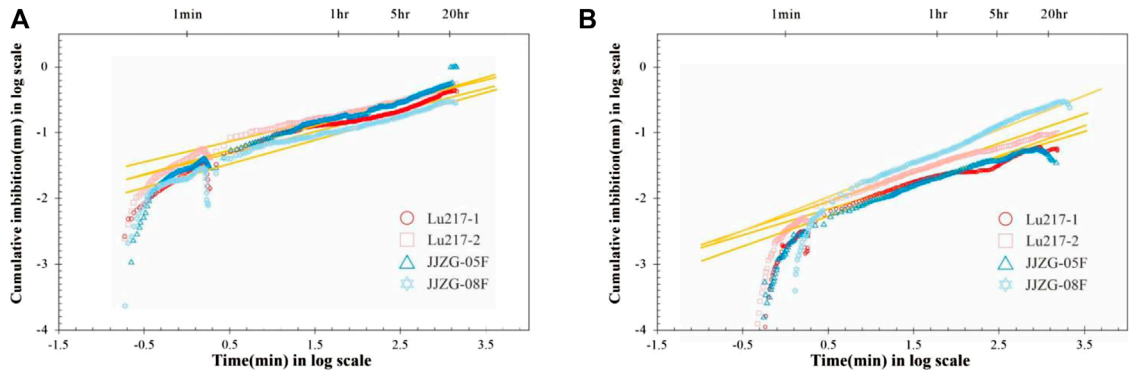

FIGURE 11
(A) Spontaneous imbibition results of deionized water from tuffaceous shale samples of the Upper Triassic Yanchang and Middle Permian Jingjingzigou Formations; **(B)** spontaneous imbibition results of n-decane from tuffaceous shale samples of the Upper Triassic Yanchang and Middle Permian Jingjingzigou Formations.

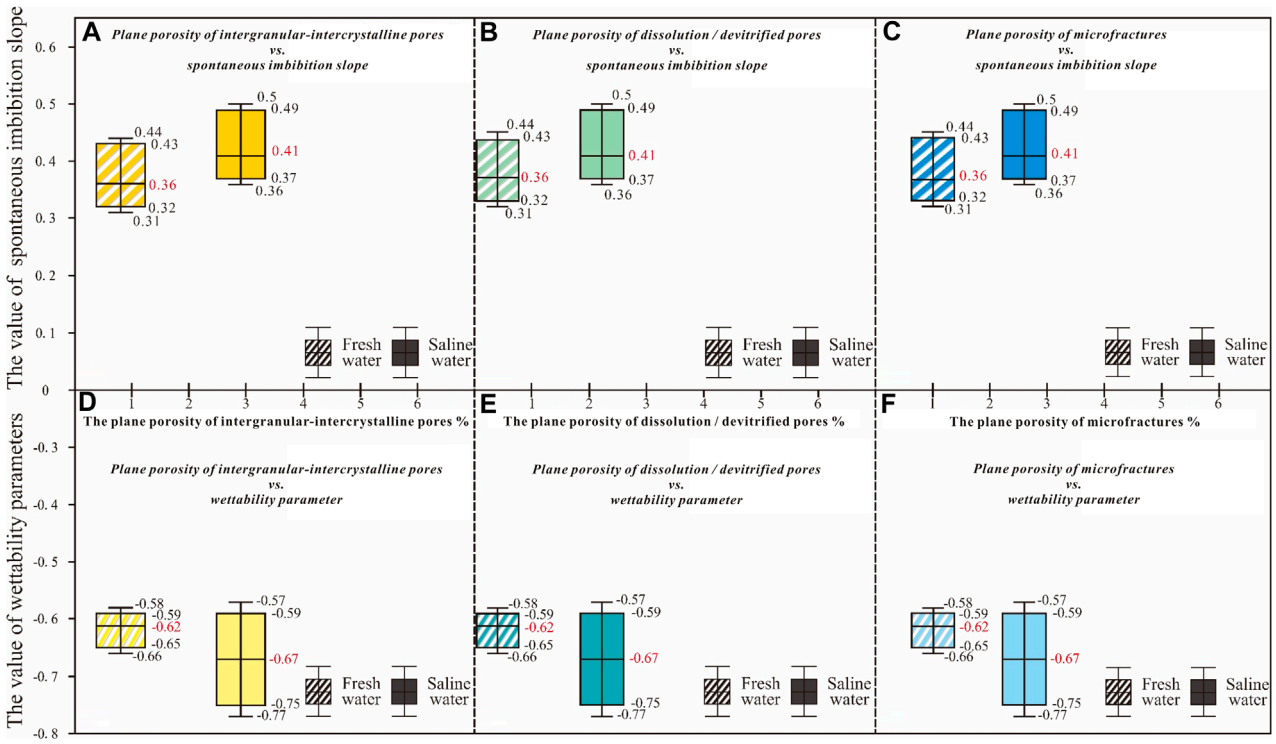

FIGURE 12
Box-plots exhibiting the correlation relationship between spontaneous imbibition slopes/wettability parameters and plane porosity of pores and microfractures under fresh-water and saline lacustrine environments, respectively. **(A–C)** Box-plots showing the correlation between spontaneous imbibition slopes and the plane porosity of intergranular-intercrystalline pores, dissolution/devitrified pores, and microfractures. **(D–F)** Box-plots showing the correlation between wettability parameters and the plane porosity of intergranular-intercrystalline pores, dissolution/devitrified pores, and microfractures.

liquid-solid interface, meanwhile, the various types of pores formed by devitrified effect led to similar capillary force in the reservoir, which is favorable for oil retention, so that the wettability of the tuffaceous shale interface is changed from hydrophilic to oleophilic, which provides effective transport channels for hydrocarbon fluids. In contrast, the Upper Triassic Yanchang Formation tuffaceous shales are subject to a low degree of devitrification, which still retains a large amount of hydrophilic components such as vitreous matter in the tuff, with less formation of devitrification pores and difficulty for hydrocarbon fluids to enter into, making the degree of interfacial wettability changed limited. The water contact angle (Figures 7d–g) of the Middle Permian Jingjingzigou Formation tuffaceous shale samples is approximately equal to that of the Upper Triassic Yanchang Formation tuffaceous shale samples (Figures 7a–c), and the oil contact angle (Figures 7d'–g') of the Middle Permian Jingjingzigou Formation tuffaceous shale samples is smaller than that of the Upper Triassic Yanchang Formation tuffaceous shale samples (Figures 7a'–c'), indicating that

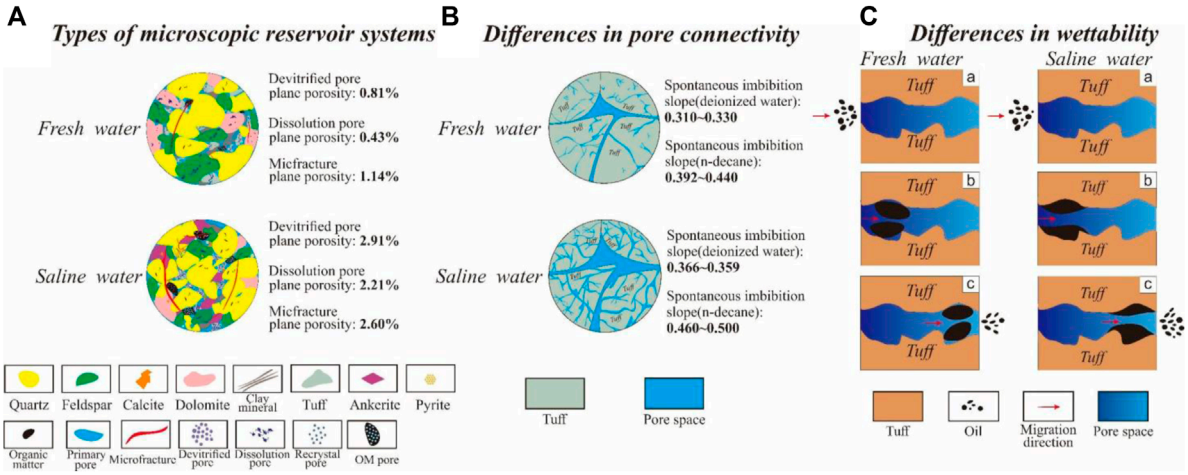

FIGURE 13
Comprehensive and conceptual schemes illustrating the effects of differential devitrification on reservoir-forming processes in the fresh-water and saline lacustrine environments, especially concerning **(A)** the types of microscopic reservoir systems, **(B)** the differences in pore connectivity, and **(C)** the differences in wettability, respectively.

the Middle Permian Jingjingzigou Formation tuffaceous shales are more oleophilic. According to the wettability parameters of each sample and the wettability classification criteria, the Middle Permian Jingjingzigou Formation samples are more oil-wettable and the Upper Triassic Yanchang Formation samples are water-wettable (Figure 8). Based on the statistical results of the spontaneous imbibition and wettability parameters of the Middle Permian Jingjingzigou Formation tuffaceous shales and the Upper Triassic Yanchang Formation tuffaceous shales (Table 3), combined with the plane porosity of the three types of pores affected by devitrification (devitrified pores, dissolution pores and microfractures) of the Middle Permian Jingjingzigou Formation tuffaceous shales and the Upper Triassic Yanchang Formation tuffaceous shales, it is obvious that the higher the value of the plane porosity, the higher the value of the spontaneous imbibition slope and the smaller the value of the wettability parameter. Moreover, all three types of pores affected by devitrification reflect the same pattern and regularity (Figure 12). The higher the degree of devitrification and the more developed the devitrification pores are, the better the pore connectivity of the tuffaceous shales, the more oleophilic the sample is, which is more favorable to the tuff-bearing reservoir space for oil and gas storage. Therefore, the difference of devitrification has a significant influence on the pore structure characteristics and interfacial wettability. The interfacial wettability of tuffaceous shales media of the Middle Permian Jingjingzigou Formation is more inclined to oil wetting than that of tuffaceous shales media of the Upper Triassic Yanchang Formation due to the difference in the degree of devitrification.

5.3 Comprehensive model of reservoir differentiation between fresh-water and saline lacustrine tuffaceous shale formation

Based on the analysis of the mineral composition, pore type, pore connectivity characteristics and interfacial wettability of the Upper Triassic Yanchang Formation and Middle Permian Jingjingzigou Formation samples, it provides clues to the degree of devitrification in two different environments, fresh-water and saline lacustrine basins, inferring that devitrification differences affect the pore structure and interfacial wettability within the reservoir. To better understand the effect of the difference in the degree of devitrification on reservoir pore connectivity and interfacial wettability as well as reservoir formation differences, a conceptual schemes of the two sets has been proposed (Figure 13).

The tuffaceous shales of the Upper Triassic Yanchang Formation differ significantly from the tuffaceous shales of the Middle Permian Jingjingzigou Formation in terms of reservoir formation mode. The low degree of devitrification in the tuffaceous shale samples of the Upper Triassic Yanchang Formation makes the devitrification pores formed in the tuff few and dispersed, mostly isolated pores. The dissolution is weak, forming fewer dissolution pores. Few microfractures, many isolated pores lack the communication of microfractures, which make it difficult for microfractures to form an effective pore network with primary pores, devitrified pores and dissolved pores, thus poor pore connectivity within the reservoir. The weak devitrified degree leads to the high content of vitreous matter in the reservoir, low pore development, restricted interfacial wettability change, as well as poor mobility of hydrocarbon fluids in the pore space of devitrified genesis. Therefore, the low degree of devitrification has little effect on the pore structure characteristics of tuffaceous shales and the wettability modification of the interface.

The Middle Permian Jingjingzigou Formation tuffaceous shales have a high degree of devitrified action, with a large number of devitrified pores formed in the tuff component. Tuffaceous shales are subject to obvious dissolution, which can further develop devitrification pores. Microfractures are well developed in tuff reservoirs subject to obvious devitrification, which can be used as effective fluid percolation channels, forming an effective pore network with primary pores, devitrification pores and dissolution pores in the reservoir. The pore connectivity gradually becomes better. The high degree of devitrification leads to high content of feldspathic quartzite in the reservoir, the development of pore space, the large reduction of

hydrophilic minerals such as vitrinite, and the significant improvement of interfacial wetting effect. Hydrocarbon fluids can flow in the pore space formed by tuff devitrification. The wetting of the fluid-rock interface in the reservoir with a high degree of devitrification has an obvious reversal, which is gradually oleophilic and facilitates the retention of hydrocarbon substances such as shale oil, which also helps the reversal of the wetting of the mixed tuffaceous shales medium interface. Therefore, the high degree of devitrification has a significant effect on the pore structure characteristics of tuffaceous shales and the wettability of the interface.

6 Conclusion

On the basis of our results from whole-rock mineral compositional constraints, FE-SEM observation and ImageJ software image extraction, spontaneous imbibition measurements, contact angle tests for surface wettability assessment and interpretation, this current work aims to provide a good opportunity for comparative investigations on the differential behaviors of microscopic pore development, pore-microfracture connectivity, interface wettability, and movable fluid storage capacity between the fresh-water and saline lacustrine tuffaceous shale reservoirs. The achievements lend new insights into the impacts of devitrification on reservoir-forming mechanism and petrophysical quality properties for the continental fine-grained mixed sedimentary systems. The following conclusions have been drawn:

(1) Compared with the Yanchang Formation of the Upper Triassic in the Ordos Basin, the tuffaceous shales the Middle Permian Jingjingzigou Formation in the Junggar Basin characterized by well-developed intergranular-intercrystalline and dissolution pores, as well as inorganic microfractures, generally yield a higher plane porosity of representative pore-fracture spaces and spontaneous imbibition slopes, a relatively lower average of n-decane contact angles and corresponding wettability parameters. It is worth noting that the coupling relationship between pore/microfracture plane porosity and spontaneous imbibition and wettability indicators are also unraveled, suggesting the saline lacustrine environment is more favorable. Nonetheless, due to the limitation in the amount of core samples of tuffaceous shales, further research is needed to examine the precision and accuracy of pore-microfracture connectivity and interface wettability, and to better assess and fully understand the microscopic reservoir heterogeneity of tuffaceous shales developed in saline lacustrine settings.

(2) We suspected that the tuffaceous shales developed in saline lacustrine settings have undergone a stronger devitrification resulting in a higher amount of devitrification and associated dissolution pores, and a relatively better connectivity between isolated micropore systems with adjacent microfractures. This would significantly facilitate the interface wettability reversal and occurrence of movable hydrocarbon fluid in microscopic reservoir spaces.

(3) Finally, a comprehensive and conceptual model is established illustrating the effects of differential devitrification on reservoir-forming patterns concerning tuffaceous shales developed in the fresh-water and saline lacustrine settings, respectively. This contribution can provide new context and perspective for seeking the root causes of *in-situ* oil movability and accumulation of the saline lacustrine tuffaceous shale reservoirs, and lay the foundation for guiding efficient exploration of continental fine-grained mixed sedimentary sequences.

Data availability statement

The raw data supporting the conclusions of this article will be made available by the authors, without undue reservation.

Author contributions

WY: Conceptualization, Investigation, Writing–original draft. BS: Conceptualization, Investigation, Writing–review and editing. ZZ: Data curation, Formal Analysis, Funding acquisition, Methodology, Project administration, Resources, Supervision, Validation, Visualization, Writing–review and editing. RZ: Formal Analysis, Project administration, Validation, Writing–review and editing. HdH: Data curation, Formal Analysis, Project administration, Writing–review and editing. ZL: Resources, Visualization, Writing–original draft. MD: Formal Analysis, Methodology, Project administration, Writing–review and editing. HwH: Project administration, Validation, Visualization, Writing–review and editing. FF: Resources, Visualization, Writing–review and editing. MX: Resources, Visualization, Writing–review and editing .

Funding

The author(s) declare that no financial support was received for the research, authorship, and/or publication of this article. This work was mainly financed by the Open Project Fund of State Key Laboratory of Shale Oil and Gas Enrichment Mechanisms and Effective Development, Sinopec Petroleum Exploration and Production Research Institute (Grant. G5800-20-ZS-KFGY004), the Natural Science Foundation of China (Grant No. 42172140), and the Science Foundation for Distinguished Young Scholars of China University of Petroleum - Beijing (No. 2462020QNXZ004).

Conflict of interest

Author RZ was employed by China Petroleum & Chemical Corporation.

The remaining authors declare that the research was conducted in the absence of any commercial or financial relationships that could be construed as a potential conflict of interest.

Publisher's note

References

Camp, W. K. (2017). Strategies for identifying organic matter types in SEM. *Am. Assoc. Petroleum Geol. Search Discov.*, 70233.

Chen, T., and Xie, Q. (2005). From optical microscopy to electron microscopy: nanogeoscience. *J. Hefei Univ. Technol.* (09), 126–1129. doi:10.3969/j.issn.1003-5060.2005.09.036

Chen, X., Li, J., Liang, H., Luo, Q., Fan, T., He, R., et al. (2014). Hydrocarbon accumulation elements analysis of tiaohu tuff reservoir of Middle permian, santanghu basin. *Xinjiang Pet. Geol.* 35 (4), 386–390.

Desmastes, D., Grosheny, D., Beaudoin, B., Gardin, S., and Gauthier, L. F. (2007). High resolution stratigraphic record constrained by volcanic ash beds at the Cenomanian—turonian boundary in the Western Interior. Basin, USA. *Cretac. Res.* 28 (4), 561–582. doi:10.1016/j.cretres.2006.08.009

Dou, W., Liu, L., Wu, K., Xu, Z., Liu, X., and Feng, X. (2018). Diagenetic heterogeneity, pore throats characteristic and their effects on reservoir quality of the Upper Triassic tight sandstones of Yanchang Formation in Ordos Basin, China. *Mar. Petroleum Geol.* 98, 243–257. doi:10.1016/j.marpetgeo.2018.08.019

Fan, B., Jin, Y., Shi, L., Li, Y., and Chen, W. (2021). Shale oil exploration potential in central Ordos Basin:A case study of Chang 7 lacustrine shale. *Oil Gas Geol.* 42 (05), 1078–1088. doi:10.11743/ogg20210506

Fan, B., Shi, L., Yang, J., Su, S., Ma, R., Yuan, Y., et al. (2022). Sedimentary environment of lacustrine organic matter in the central Ordos Basin. *Oil Gas Geol.* 43 (03), 648–657. doi:10.11743/ogg20220313

Fu, J., Li, S., Niu, X., Deng, X., and Zhou, X. (2020). Geological characteristics and exploration of shale oil in Chang 7 member of triassic Yanchang Formation, Ordos Basin, NW China. *Petroleum Explor. Dev.* 47 (05), 931–945. doi:10.1016/s1876-3804(20)60107-0

Fu, J., Luo, S., Niu, X., Lu, Q., Xu, L., Feng, S., et al. (2015). Sedimentary characteristics of channel type gravity flow of the member 7of Yanchang Formation in the longdong area, Ordos Basin. *Bull. Mineralogy, Petrology Geochem.* 34 (01), 29–37+1. doi:10.3969/j.issn.1007-2802.2015.01.003

Fu, Q., Sun, X., and Liu, Y. (2009). Geologic significance and Re-establishment of basin character in late triassic of Ordos Basin. *J. Tongji Univ.* 37 (11), 1537–1540. doi:10.3969/j.issn.0253-374x.2009.11.023

Gao, F., Wang, C., Song, Y., Chen, Z., Liu, Q., Li, Z., et al. (2021). Ar-ion polishing FE-SEM analysis of organic maceral identification. *Petroleum Geol. Exp.* 43 (02), 360–367. doi:10.11781/sysydz202102360

Gao, Z., and Hu, Q. (2016). Initial water saturation and imbibition fluid affect spontaneous imbibition into Barnett shale samples. *J. Nat. Gas Sci. Eng.* 34, 541–551. doi:10.1016/j.jngse.2016.07.038

Gao, Z., Liang, Z., Jiang, Z., Xiong, S., Duan, L., Yang, B., et al. (2022). A method and equipment for evaluating the wettability of shale reservoirs. *China Natl. Intellect. Prop. Off.*

Gu, L., and Li, J. (2020). The focused ion beam (FIB) technology and its applications for earth and planetary sciences. *Bull. Mineralogy, Petrology Geochem.* 39 (06), 1119–1066. doi:10.19658/j.issn.1007-2802.2020.39.102

Guan, Q., Dong, D., Wang, S., Huang, J., Wang, Y., Zhang, C., et al. (2016). Analyses on differences of microstructure between marine and lacustrine facies shale reservoirs. *Nat. Gas. Geosci.* 27 (3), 524–531. (in Chinese with English Abstract). doi:10.11764/j.issn.1672-1926.2016.03.0524

Jiang, Z. (2019). *Influence of volcanic ash on Source rock organic matter enrichment in the Lucaogou Formation, the Jimusar Depression*. Master Thesis: China University of Petroleum. (in Chinese with English Abstract).

Kirov, G., Šamajova, E., Nedialkov, R., and Stanimirova, T. (2011). Alteration processes and products of acid pyroclastic rocks in Bulgaria and Slovakia. *Clay Miner.* 46 (2), 279–294. doi:10.1180/claymin.2011.046.2.279

Li, C., Li, Y., Chen, X., Liu, Z., Li, P., and Wang, Y. (2020). Pore characterization of the Permian shale in the Wuhu area using FE-SEM technique. *J. Chin. Electron Microsc. Soc.* 39 (02), 151–157. doi:10.3969/j.issn.1000-6281.2020.02.009

Li, D. (2004). Return to petroleum geology of Ordos Basin. *Petroleum Explor. Dev.* (06), 1–7. doi:10.0000/1000-0747-31-942

Li, Y., Xu, X., Zhang, J., Chen, S., Bai, J., Liu, W., et al. (2022). Hybrid sedimentary conditions of organic - rich shales in faulted lacustrine basin during volcanic eruption episode: a case study of shahezi formation (K,*sh* Fm.), lishu faulted depression, south songliao basin. *Earth Sci.* 47 (5), 1728–1747. doi:10.3799/dqkx.2022.015

Liang, X., Jin, Z., Liu, Q., Shpilman, A., Li, P., Morozov, V., et al. (2021). Influence of volcanic ash on the formation of organic-rich shale—an example from the mesozoic bazhenov Formation in the west siberian basin. *Petroleum Nat. Gas Geol.* 42 (01), 201–211. doi:10.11743/ogg20210117

Liu, Q., Li, P., Jin, Z., Sun, Y., Hu, G., Zhu, D., et al. (2022a). Organic-rich formation and hydrocarbon enrichment of lacustrine shale strata: a case study of Chang 7 Member. *Sci. China Earth Sci.* 65 (1), 118–138. doi:10.1007/s11430-021-9819-y

Liu, S., Yao, M., Feng, Y., and Fan, T. (2018). Influencing factor analysis of devitrification pore and its relationship with hydrocarbon in tiaohu Formation of malang depression. *Special Oil Gas Reservoirs* 25 (01), 16–19. doi:10.3969/j.issn.1006-6535.2018.01.004

Liu, X., Jiang, Z., Yuan, X., Chen, C., and Wang, C. (2022b). Influence of the Cretaceous fine-grained volcanic materials on shale oil/gas, Luanping Basin. *Oil Gas Geol.* 43 (02), 390–406. doi:10.11743/ogg20220212

Lowe, J. D. (2011). Tephrochronology and its application: a review. *Quat. Geochronol.* 6 (2), 107–153. doi:10.1016/j.quageo.2010.08.003

Luo, J., Tian, J., Ma, J., Yan, J., Liang, Y., and Hu, Z. (2022). Sedimentary environment and organic matter enrichment mechanism of Permian Lucaogou Formation in Jiye-1 well area, Jimsar Sag. *Lithol. Reserv.* 34 (5), 73–85. doi:10.12108/yxyqc.20220506

Lv, P., Li, M., Yang, Z., Lin, M., Dong, C., and Peng, B. (2015). Review of the influencing factors of reservoir wettability. *Sci. Technol. Eng.* 15 (25), 88–94. doi:10.3969/j.issn.1671-1815.2015.25.016

Ma, J., Hung, Z., Liu, Z., Chen, C., and Gao, X. (2015). Tight reservoir characteristics of sedimentary organic matter-bearing tuff in Tiaohu Formation of Santanghu Basin. *Earth Sci. Front.* 22 (6), 185–196. doi:10.13745/j.esf.2015.06.014

Macquaker, J., and Davies, S. (2008). Lithofacies variability in fine-grained mixed clastic carbonate successions: implications for identifying shale-gas reservoir. *AAPG.*

Marquez, X. M., and Mountjoy, E. W. (1996). Microfractures due to overpressures caused by thermal cracking in well-sealed Upper Devonian reservoirs, deep Alberta Basin. *AAPG Bull.* 80 (4), 570–588. doi:10.1306/64ed884a-1724-11d7-8645000102c1865d

Marshall, R. R. (1961). Devitrification of natural glass. *Geol. Soc. Am. Bull.* 72, 1493–1520. doi:10.1130/0016-7606(1961)72[1493:dong]2.0.co;2

Mastalerz, M., Schimmelmann, A., Drobniak, A., and Chen, Y. (2013). Porosity of Devonian and Mississippian New Albany Shale across a maturation gradient: insights from organic petrology, gas adsorption, and mercury intrusion. *AAPG Bull.* 97 (10), 1621–1643. doi:10.1306/04011312194

Mchenry, L. J. (2009). Element mobility during zeolitic and argillical teration of volcanic ash in a closed-basin lacustrine environment: case study Olduvai Gorge, Tanzania. *Chem. Geol.* 265, 540–552. doi:10.1016/j.chemgeo.2009.05.019

Nan, J., Wang, S., Yao, W., and Lu, Y. (2007). Micro-fractures in extra low permeability reservoir of Yanchang Formation in Ordos Basin. *Lithol. Reserv.* 19 (4), 40–44. doi:10.3969/j.issn.1673-8926.2007.04.007

Nickel, E. H., and Grice, J. D. (1998). The IMA commission on new minerals and mineral names: procedures and guidelines on mineral nomenclature. *Can. Mineralogist* 36, 10–20. doi:10.1007/BF01226571

Pan, Y., Huang, Z., Guo, X., Li, T., Fan, T., and Xu, X. (2022). Analysis of accumulation conditions of lacustrine organic-rich shale oil affected by volcanic ash: a case study of the Lucaogou Formation in the Tiaohu-Malang sag, Santanghu basin. *Acta Geol. Sin.* 96 (3), 1053–1068. doi:10.19762/j.cnki.dizhixuebao.2021140

Qiu, L., Jiang, Z., Chen, W., Li, X., and Xiong, Z. (2002). A new type of secondary porosity—quartz dissolution porosity. *Acta Sedimentol. Sin.* (04), 621–627. doi:10.3969/j.issn.1000-0550.2002.04.014

Qiu, X., Liu, C., Mao, G., Deng, Y., Wang, F., and Wang, J. (2015a). Major, trace and platinum-group element geochemistry of the upper Triassic nonmarine hot shales in the Ordos basin, Central China. *Appl. Geochem.* 53, 42–52. doi:10.1016/j.apgeochem.2014.11.028

Qiu, X., Liu, C., Wang, F., Deng, Y., and Mao, G. (2015b). Trace and rare earth element geochemistry of the Upper Triassic mudstones in the southern Ordos Basin, Central China. *Geol. J.* 50 (4), 399–413. doi:10.1002/gj.2542

Schembre, J. M., Tang, G., and Kovscek, A. R. (2006). Wettability alteration and oil recovery by water imbibition at elevated temperatures. *J. Petroleum Sci. Eng.* 52, 131–148. doi:10.1016/j.petrol.2006.03.017

Stinco, L., and Barredo, S. (2021). Geomechanics and electrofacies characterization of the los molles formation (lower to Middle jurassic), Neuquén Basin. *J. S. Am. Earth Sci.* 110, 103338. doi:10.1016/j.jsames.2021.103338

Tang, X., Zhang, J., Jin, Z., Xiong, J., Lin, L., Yu, Y., et al. (2015). Experimental investigation of thermal maturation on shale reservoir properties from hydrous pyrolysis of Chang 7 shale, Ordos Basin. *Mar. Petroleum Geol.* 64, 165–172. doi:10.1016/j.marpetgeo.2015.02.046

Tian, H., Fan, M., Victor, V., Chamberlain, K., Waite, L., Stern, J. R., et al. (2022). Rapid early Permian tectonic reorganization of Laurentia's plate margins: evidence from volcanic tuffs in the Permian Basin, USA. *Gondwana Res.* 111, 76–94. doi:10.1016/j.gr.2022.07.003

Tian, Y., Zhong, J., Wang, S., Tao, H., Liu, S., Li, Y., et al. (2015). Seismites and their geological significances of the triassic Yanchang Formation in fuxian exploration area, Ordos Basin. *J. Palaeogeogr.* 17 (04), 541–552. doi:10.7605/gdlxb.2015.04.044

Tomaru, H., Lu, Z., Fehn, U., and Muramatsu, Y. (2009). Origin of hydrocarbons in the Green Tuff region of Japan: ^{129}I results from oil field brines

and hot springs in the Akita and Niigata Basins. *Chem. Geol.* 264, 221–231. doi:10.1016/j.chemgeo.2009.03.008

Wang, C., Wang, Q., Chen, G., He, L., Xu, Y., Chen, L., et al. (2017a). Petrographic and geochemical characteristics of the lacustrine black shales from the upper Triassic Yanchang formation of the Ordos basin, China: implications for the organic matter accumulation. *Mar. Petroleum Geol.* 86, 52–65. doi:10.1016/j.marpetgeo.2017.05.016

Wang, D., Bltler, R., Zhang, J., and Seright, R. (2012). Wettability survey in Bakken shale with surfactant-formulation imbibition. *SPE Reserv. Eval. Eng.* 15 (06), 695–705. doi:10.2118/153853-pa

Wang, F., and Guo, S. (2019). Influential factors and model of shale pore evolution: a case study of a continental shale from the Ordos Basin. *Mar. Petroleum Geol.* 102, 271–282. doi:10.1016/j.marpetgeo.2018.12.045

Wang, G., Jin, Z., Zhang, Q., Zhu, R. K., Tang, X., Liu, K. Q., et al. (2023b). Effects of clay minerals and organic matter on pore evolution of the early mature lacustrine shale in the Ordos Basin, China. *J. Asian Earth Sci.* 246, 105516. doi:10.1016/j.jseaes.2022.105516

Wang, G., Li, D., Liu, L., Dou, Y., and Zheng, Q. (2021). Production analysis and influencing factors of igneous reservoir in northwest margin of Junggar Basin. *Bull. Sci. Technol.* 37 (03), 9–15+21. doi:10.13774/j.cnki.kjtb.2021.03.002

Wang, J., Bao, Z., Chen, M., Sun, F., Liu, R., Zhao, M., et al. (2005). Differention of sandstones tuff fillings and its effect on porosity—an example from the paleozoic sandstones in northwestern Ordos. *Chin. J. Geol.* (03), 429–438. doi:10.3321/j.issn:0563-5020.2005.03.012

Wang, J., Liu, C., Li, H., Wu, T., and Wu, J. (2017b). Geochronology, potential source and regional implications of tuff intervals in chang-7 member of Yanchang Formation, south of Ordos Basin. *Acta Sedimentol. Sin.* 35 (04), 691–704. doi:10.14027/j.cnki.cjxb.2017.04.004

Wang, J., Yuan, B., Liu, J., Li, Y., Li, E., Ma, C., et al. (2022). Genesis and pore development characteristics of permian Lucaogou migmatites, jimsar sag, Junggar Basin. *Petroleum Geol. Exp.* 44 (03), 413–424. doi:10.11781/sysydz202203413

Wang, R., and Sun, W. (2009). A study on micro cracks in super low permeability sandstone reservoir of the Upper Triassic Yanchang Formation in the Ordos Basin. *Geol. Rev.* 55 (3), 444–448. doi:10.3321/j.issn:0371-5736.2009.03.016

Wang, X. (2017). *Stratigraphic framework and sedimentary evolution of the Permian-Jurassic in the surrounding area of the Bogda Mountains*. East China: China University of Petroleum.

Wang, X., Zhang, X., Li, S., Zhang, J., and Zhang, Z. (2023a). Redox sensitive trace element compositions of the Shuinan Formation black shale in the Laiyang Sag: controlling factors of organic matter enrichment. *Geoscience* 37 (3), 733–744. (in Chinese with English Abstract). doi:10.19657/j.geoscience.1000-8527.2021.153

Wood, J. M., Sanei, H., Curtis, M. E., and Clarkson, C. R. (2015). Solid bitumen as a determinant of reservoir quality in an unconventional tight gas siltstone play. *Int. J. Coal Geol.* 150-151, 287–295. doi:10.1016/j.coal.2015.03.015

Wu, K., Zha, M., Wang, X., Qu, J., and Chen, X. (2005). Further researches on the tectonic evolution and dynamic setting of the Junggar Basin. *Acta Geosci. Sin.* (03), 217–222. doi:10.3321/j.issn:1006-3021.2005.03.004

Wu, Q. (1986). An overview of the developmental stages, tectonic units and local tectonic genesis of the Junggar Basin. *Xinjiang Pet. Geol.* (01), 29–37.

Yang, H., Chen, L., and Kong, Y. (2004). A novel classification of structural units in Junggar Basin. *Xinjiang Pet. Geol.* (06), 686–688. doi:10.3969/j.issn.1001-3873.2004.06.034

Yang, S., Hu, W., Wang, X., Jiang, B., Yao, S., Sun, F., et al. (2019). Duration, evolution, and implications of volcanic activity across the Ordovician–Silurian transition in the Lower Yangtze region, South China. *Earth Planet. Sci. Lett.* 518, 13–25. doi:10.1016/j.epsl.2019.04.020

Yang, W., Wang, Q., Song, Y., Jiang, Z., Meng, W., Liu, G., et al. (2020). New scaling model of the spontaneous imbibition behavior of tuffaceous shale: constraints from the tuff-hosted and organic matter-covered pore system. *J. Nat. Gas Sci. Eng.* 81, 103389. doi:10.1016/j.jngse.2020.103389

Yang, Y., Song, C., and He, S. (2015). Jurassic tectonostratigraphic evolution of the Junggar basin, NW China: a record of Mesozoic intraplate deformation in Central Asia. *Tectonics* 34 (1), 86–115. doi:10.1002/2014tc003640

Yao, J., Deng, X., Zhao, Y., Han, T., Chu, M., and Pang, J. (2013). Characteristics of tight oil in triassic Yanchang Formation, Ordos Basin. *Petroleum Explor. Dev.* 40 (02), 161–169. doi:10.1016/s1876-3804(13)60019-1

Yao, Y., and Liu, D. (2009). Microscopic characteristics of microfractures in coals: an investigation into permeability of coal. *Procedia Earth Planet. Sci.* 1 (1), 903–910. doi:10.1016/j.proeps.2009.09.140

Ye, H., Ning, Z., Wang, Q., Cheng, Z., Huang, L., and Mu, D. (2019). Spontaneous imbibition experiment and wettability of shale reservoir. *Fault-Block Oil Gas Field* 26 (01), 84–87. doi:10.1016/j.epsl.2019.04.020

Zhang, G., Zou, C., Zhu, R., Yuan, X., and Zhao, X. (2010). Petroleum geology and exploration for volcanic reservoirs in the sedimentary basins of China. *Strategic Study CAE* 12 (5), 30–38. doi:10.3969/j.issn.1009-1742.2010.05.005

Zhang, J. (1982). Tectonic evolution of Ordos Basin and its oil and gas potential. *Oil Gas Geol.* (04), 304–315. doi:10.11743/ogg19820411

Zhang, L., Li, J., Song, Y., Chen, S., Lu, J., Guo, J., et al. (2021a). Gas accumulation characteristics and exploration potential of the Carboniferous volcanic rocks in Junggar Basin. *China Pet. Explor.* 26 (6), 141–151. doi:10.3969/j.issn.1672-7703.2021.06.010

Zhang, Z., Feng, J., Cai, J., Chen, K., and Meng, Q. (2021b). Driving force for spontaneous imbibition under different boundary conditions. *Chin. J. Comput. Phys.* 38 (05), 513–520. doi:10.19596/j.cnki.1001-246x.8391

Zhao, H., Huang, W., Wang, C., Di, Y., Qi, J., Xiao, Y., et al. (2009). Micropores from devitrification in volcanic rocks and their contribution to reservoirs. *Oil Gas Geol.* 30 (01), 47–52+58. doi:10.11743/ogg20090107

Zhao, W., Zhu, R., Hu, S., Hou, L., and Wu, S. (2020). Accumulation contribution differences between lacustrine organic-rich shales and mudstones and their significance in shale oil evaluation. *Petroleum Explor. Dev.* 47 (6), 1160–1171. doi:10.1016/s1876-3804(20)60126-x

Zheng, H., Sun, X., Wang, J., Zhu, D., and Zhang, X. (2018b). Devitrification pores and their contribution to volcanic reservoirs: a case study in the Hailar Basin, NE China. *Mar. Petroleum Geol.* 98, 718–732. doi:10.1016/j.marpetgeo.2018.09.016

Zhou, D., Li, M., Shi, Y., Zou, Y., and Liu, S. (2018). Sensitivity analysis of imbibition stability time in tight sandstone reservoir. *Special Oil Gas Reservoirs*. 25 (02), 125–129. doi:10.3969/j.issn.1006-6535.2018.02.025

Zhu, G., Zhang, J., Yao, G., Li, Y., Wang, X., and Yu, C. (2014a). Sedimentary volcanic dust tuff, an important kind of rock storing hydrocarbon Resources: discussion on the lithology of Middle permian Lucaogou oil-bearing rocks in the North of Xinjiang. *Mar. Orig. Pet. Geol.* 19 (01), 1–7. doi:10.3969/j.issn.1672-9854.2014.01.001

Zhu, R., Zou, C., Wu, S., Yang, Z., Mao, Z., Yang, H., et al. (2019). Mechanism for generation and accumulation of continental tight oil in China. *Petroleum Nat. Gas Geol.* 40 (06), 1168–1184. doi:10.11743/ogg20190602

Zhu, S., Zhu, X., Liu, Y., Chen, X., Wang, J., Wang, X., et al. (2014b). Petrological and geochemical features of dolomitic rocks in the lower permian fengcheng Formation in wuerhe—xiazijie area, Junggar Basin. *Geol. Rev.* 60 (05), 1113–1122. doi:10.16509/j.georeview.2014.05.017